Journal of Applied Fluid Mechanics, Vol. 17, No. 9, pp. 1820-1843, 2024.
Available online at www.jafmonline.net, ISSN 1735-3572, EISSN 1735-3645.
https://doi.org/10.47176/jafm.17.9.2390

Numerical Investigation and Statistical Analysis of the Flow Patterns Behind Square Cylinders Arranged in a Staggered Configuration Utilizing the Lattice Boltzmann Method

M. Abid[1], N. Yasin[2], M. Saqlain[3†], S. Ul-Islam[4] and S. Ahmad[5]

[1] *Department of Mathematics, North Carolina State University, NC 27695, Raleigh, USA*
[2] *Departments of Mathematics & Statistics, Old Dominion University, VA 23529, Norfolk, USA*
[3] *Department of Mathematics, King Mongkut's University of Technology, Thonburi, 10140, Bangkok, Thailand*
[4] *Departments of Mathematics, COMSATS University, Islamabad 44000, Islamabad, Pakistan*
[5] *School of Energy and Power Engineering, Jiangsu University, 212013 Zhenjiang, China*

†Corresponding Author Email: Muhammad.saql@kmutt.ac.th

ABSTRACT

Flow past bluff bodies like square cylinders is important in engineering applications, but flow patterns behind staggered cylinder arrangements remain poorly understood. Existing studies have focused on tandem or side-by-side configurations, while offset orientations have received less attention. The aim of this paper is to numerically investigate flow dynamics and force characteristics behind two offset square cylinders using the single relaxation time lattice Boltzmann method. The effects of changing both the Reynolds number (Re = 1-150) and gap spacing ratio (g* = 0.5-5) between the cylinders are analyzed. Instantaneous vorticity contours, time histories of drag and lift coefficients, power spectra of lift, and force statistics are used to characterize the flow. Different flow regimes have been identified in various ranges of Re and g* - including steady, chaotic, flip-flopping, single-bluff body, and fully developed flows. Larger spacings led to more regular vortex dynamics and force statistics. Smaller spacings promoted complex interactions and modulated forces. Offset cylinder orientation and spacing significantly influence flow features in staggered arrangements. The findings provide new modalities for controlling fluid dynamics past bluff bodies by tuning Re and gap parameters.

Article History

Received. October 23, 2023
Revised. March 17, 2024
Accepted. April 7, 2024
Available. online July 2, 2024

Keywords:

Lattice Boltzmann Method
Computational Fluid dynamics
Statistical Analysis
Analysis of forces
Numerical Analysis
Vortex shedding frequency

1. INTRODUCTION

The fluid dynamics features and instability of the wake structure mechanism behind complex bluff bodies of different cross sections plays a key role in engineering problems and researchers are attracted to this field due to its practical importance. Proximity in multiple cylinders increases complication in problems due to interaction in wakes galloping and shear layers. We can encounter daily life examples such as bridges, heat exchanger tubes, offshore structures, transmission cables, and smokestack to understand the practical usefulness of flow past bluff bodies. In previous research, flow past circular cylinders have been regularly encountered. In various engineering applications, square structure serves a vital role among different bluff structures.

In most of our problems we used dimensionless number known as Reynolds number ($Re = U_\infty d/v$), which shows the uniform inflow type of velocity is the U_∞, d represents the diameter of the structure and v describes the viscosity that named kinematic) to analyze flow behavior around cylinders. Tong et al. (2015) numerically methodology of investigated flow behind both cylinders like staggered circular and observed change in pressure distribution at different incident angles (α), smaller drag force ($C_D = 2F_D/\rho U_\infty^2$, where F_D shows the special force towards the direction like a stream wise and ρ is represents the density) is observed at low alignment angles as compared to single cylinder and high alignment angles. A study on flow induced vibrations and characteristics was conducted by Kim and Alam (2015) on two adjacent cylinders arrangements by using single sheets. They observed four distinct vibrations patterns at different intervals of separation ratio ($g^* = s/d$, here s represents the distance among the cylinders accordingly to surface to surface) and analyzed that fluid-structure interaction

contrasting elastic and fixed cylinder are not same. Furquan and Mittal (2015) studied flow over square cylinders by varying flexibility of splitter plate positioned side by side and found that natural structure frequency is lower than the frequency of out of phase vibrations. Octavianty and Asai (2016) examined that attaching short length splitter plate to two side-by-side square cylinders can reduce sound level of sound pressure and if we attach short spanwise length splitter plate to cylinders in staggered array then antiphase vortex shedding and in-phase sound radiation will be dominating.

Wake behind two staggered cylinders is experimentally analyzed by Alam et al. (2016) at $Re = 1.3 \times 10^4$ and found four different flow regimes and they also discuss the physical aspect of flow to initial conditions and Strouhal numbers ($St = f_s d/U_\infty$, here f_s translates the frequency for shedding style vortex). A computational investigation of incompressible flow behind two parallel cylinders was conducted by Singha et al. (2016) because of using unstructured finite volume method (FVM) Rehman et al. (2021) and Abdulaziz et al. (2022) at low Re $(20 \leq Re \leq 160)$ and find different types of flow regimes for unsteady and steady flow. Vu et al. (2016) compared numerically the flow characteristic behind two different cylinders at next to each other and tandem arrangement by varying Re and g^* and they also observed vortex shedding, C_D and pressure distribution behind both arrangements. Liu and Jaiman (2016) studied gap flow effect on vortex that induced vibration of circular cylinders at parallel to one another. Baranwal and Chhabra (2016) studied numerically free convection heat transfer in power law fluids from cold and heated cylinders set up in two-dimensional (2D) flow regimes side by side. Flow that regimes past two staggered types of square cylinders are numerically simulated at fixed values of Re and varying separation ratio from 0.1 to 6 by Aboueian and Sohankar (2017) using FVM and observed that upstream cylinder (C_1) experienced smaller C_D than the downstream cylinder (C_2). Hsu et al. (2017) use spectral element method to determine the flow regimes over two staggered cylinders array at low Re $(Re = 100 - 800)$ by varying g^* and α. Griffith et al. (2017) give a thorough analysis of the dynamic response of elastically mounted cylinders in various arrangements (staggered and tandem) in free-stream flow at fixed Re = 200.

The flow pattern behind two circular cylinders numerically studied at low Re from 40 to 200 at various rotation by Dou et al. (2018). They observed that length of the wake become shorter with increasing in Re. Wu et al. (2018) applied lattice Boltzmann of type immersed boundary to flux to examine the flow characteristics at laminar regime. Zhang et al. (2018) used lattice Boltzmann method (LBM) simulations to know about flow interference past two circular cylinders by keeping one cylinder fixed and forced second one to vibrate in crosswise direction at fixed $Re = 100$ and noticed different role of response state, oscillating frequency and pitch ratio. Heat transfer and fluid dynamics behavior is numerically investigated at incidence past two square cylinders at fixed $Re = 100$ and differing α from 0° to 45° with step size of 5° by Patel et al. (2018). They observed maximum heat transfer at 45°. Liu and An (2018) numerically examined far-wake structure flow past two circular type cylinders that are arranged in an offset pattern at $Re = 100$. Islam et al. (2019) numerically investigated different flow behaviors with square-shaped cylinders arranged irregularly at $Re = 160$ and g^* ranges from 0 to 6 by implementing Lattice Boltzmann technique with single relaxation time (SRT-LBM).

Wu et al. (2020) numerically establish studied for the different flow past two stationary staggered cylinders at high $Re = 1.4 \times 10^5$) by varying center-to-center pitch and α from 1.5 to 4 and 0° to 90° and successfully simulated critical aerodynamics phenomena. Wake pattern in side-by-side arrangement of two vibrating cylinders using $2D$ Computational Fluid Dynamics (CFD) are numerically analyzed by Chen et al. (2019). The numerical investigation on $2D$ flow past two circular staggered cylinders at fixed $Re = 100$ with various g^* at streamwise and transverse directions are performed by Zhang et al. (2019). They analyzed intensely perturbed wake flow between centerlines and beside C_1, and the flow at downstream of both cylinder shows multiple peaks fluctuation because of complex interaction. Zhang et al. (2021) investigate the vortex-induced vibration over two staggered circular cylinders with Re ranges from 22,000 to 88,000 and varying in-line and crossflow gap. Xu et al. (2020) studied hydrodynamic-induced vibration characteristic past two flexible staggered cylinders Robichuax et al. (1999) with fixed aspect and mass ratio and varying Re and towing velocities. Vinodh and Supradeepan (2020) observed control cylinder affect with twin circular type of cylinder placed next to each other by varying control cylinder position downstream along the x-axis with fixed $Re = 100$ by using the proper method orthogonal decomposition (POD) and other is Fourier fast transform (FFT).

The experimental study of biostability phenomenon downstream around two circular finite cylinders are presented by Woyciekoski et al (2020). They used hot wire anemometry for aerodynamic channel and for hydraulic channel they examine flow visualization by injecting ink into the water. Bai et al. (2020) uses direct numerical approach with state of art special dynamic mode composition to analyzed deflected oscillatory wake pattern past two different circular round cylinders. Guo and Shu (2020) used particle image velocimetry (PIV) explore the impact of inclination α over the flow wake characteristics past two and as well as three next to each other inclined cylinders and find flip-flop gap flow, not any type of deflection over gap flow and purely deflected flow pattern for both arrangements. Sanyal and Dhiman (2020) investigate the thermal buoyancy's influence in a viscosity that is stratified flow field for a type of shear-thinning fluid passing past two heated along the square cylinders at Re ranges for 1 to 40. Energy transmission in turbulent flows past two different square cylinders stacked in tandem was investigated in numerical research by Zhou et al. (2020). The influence of dual splitter plate lengths, both in front of and behind parallel square cylinders, at a fixed Reynolds number (Re) of 150 was the focus of a later study by Zhou et al. (2021). In the investigation, 'g*' and the splitter plate length were systematically changed

between 0.5 and 5 and 1 to 5, respectively. The wake structure was significantly impacted due to the splitter plates being longer. Moreover, with a constant value of "Re" of 100 and "g^*," Zhou et al. (2021) conducted and proved a numerical study of the flow around two square cylinders in different configurations. Findings from this study demonstrated that the flow patterns of the various designs varied. In a related study, Aboueian et al. (2021) examined and showed that the flow past finite square cylinders mounted on walls (Murtaza and Ahmad 2024).

Many researchers has adopted two-dimensional computation involving numerous bluff bodies for $Re < 200$ (e.g., Furquan and Mittal (2015), $Re = 100$; Singha et al. (2016), $20 \leq Re \leq 160$; Aboueian and Sohankar (2017), $Re = 150$; Zhang et al. (2018), $Re = 100$; Patel et al. (2018), $Re = 100$; Liu and An (2018), $Re = 150$; Islam et al. (2018), $Re = 160$; Chen et al. (2019), $Re = 100$; Zhang et al. (2019), $Re = 100$). Re and spacing in our provided example range from 0 to 150 and 0.5 to 5, and two-dimensional computation is the foundation of our work in the paper. Flow past two offset square cylinders with varying Re and g^* is not available in literature. The motivation of the current work is to observe flow behavior past offset cylinders with changing Re and g^*.

Shen et al. (2021) observed the flow past two staggered circular cylinders shows rich wake patterns owing to the interactions between the shear layers from two cylinders. Understanding the wake dynamics behind two staggered cylinders is of fundamental importance for practical engineering applications such as the design of heat exchanger tube bundles. Cylinders are widely employed in engineering applications, such heat exchangers, according to Rashidi et al. (2020). Optimizing thermohydraulic performance of heat exchangers requires in-depth comprehension of the heat transfer mechanisms from cylinder arrays. Sharma et al. (2021) this paper, an attempt has been made to understand the vortex dynamics in the wake downstream of a wall-mounted square cylinder by using machine learning algorithms, namely, cluster-based reduced order modeling and long short-term memory neural networks. Veena et al. (2020) - Toward this, the flow-induced vibration characteristics of two identical square cylinders mounted elastically in tandem arrangements are numerically investigated in this paper, for a fixed upstream cylinder and a cylinder that is permitted to vibrate in the direction of crossflow. The response is found to depend significantly on the gap between the cylinders (Abid et al. 2024).

We have organized our paper as follows: description of problem, conditions for initial and boundary, and LBM for nearly incompressible NS equations is described in Section 2. The investigation of grid independence, the influence of domain for computational part, and validation of code are all presented in Section 3. Section 4 shows the computed findings, including patterns of flow, analysis of forces by time history, analysis of lift coefficient frequency spectra, also includes vorticity images at a specific instant by visualization, as well as visualization of streamlines, and force of statistics. The result discussion and including the comparison has been presented in section 5. Conclusion and final remarks are presented in Section 6.

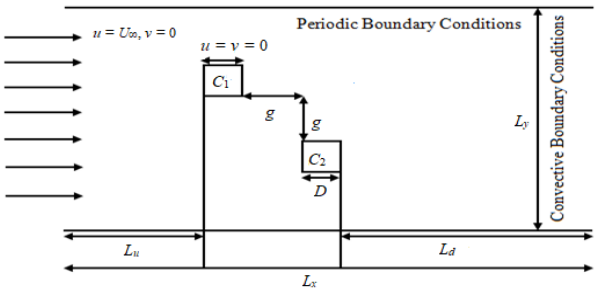

Fig. 1 Diagrammatic representation of the flow through two offset cylinders

2. PHYSICAL MODEL AND NUMERICAL STUDY

We will discuss problem geometry, initial and boundary conditions, single-relaxation-time LBM, and force evaluation in this section briefly.

2.1 Problem Geometry

The schematic picture of the simulated model is presented by the Fig. 1. Two type cylinders $C_1$and C_2 are upstream and downstream cylinders arranged offset in an unconfined channel. Both cylinders are subjected to cross flow with U_∞. The symbol ∞ is used as a subscript in U_∞ for the representation of distant values from the cylinders. g, D, Lu, Ld, Lx and Ly are the separation ratio, size of the cylinder, upstream position, downstream distance, length, and the domain's height, respectively. To make the analysis of the suggested problem computational viable, the computational domain's boundaries are located sufficiently far away from the cylinder (Saqlain et al. 2024). Constant inflow velocity is used at the position of inlet. Convective and periodic type of conditions are implemented at the exit and walls of the channel, respectively Krüger et al. (2017). No-slip conditions are used for the cylinder surfaces Mohamad (2011). The 2D flow is characterized by employing a two-dimensional coordinate system (x and y), with the x-axis side representing the streamwise way of the direction and the y-axis line representing the cross-sectional direction. After a following convergence test is satisfied, simulation is stopped.

$$\text{error} = \frac{\sqrt{\sum_{i,j}[u_{i,j}(t+1)-u_{i,j}(t)]^2}}{\sqrt{\sum_{i,j}[u_{i,j}(t+1)]^2}} \leq 5 \times 10^{-6} \quad (1)$$

To ensure appropriate time averaging simulation were run for several values in the vicinity of a million-time steps if the criteria for the convergence do not meet for the requirement. We utilize the 64-bit Fortran 90 platform to construct in-house computational code utilizing LBM. HP ProBook 450 G5 (8GB RAM, 256 GB SSD, and Intel(R) Core (TM) i5-8250U CPU @ 1.60GHz) and Haier Y11C (8GB RAM, 1TB hard disk, and Intel® Core™ M-7Y30) with Windows 10 (64-bit) system is used for computations. Vorticity and streamlines graphs are drawn by using Tecplot 360. Moreover, plots of power spectra of

C_L and history time analysis of both C_D and C_L are drawn by using MATLAB R2020a. The first few thousand simulation steps represent the transient part of the flow and are not taken into account for determining the statistical force.

2.2 The Boltzmann Lattice Method

Lattice Boltzmann equation algorithm is very simple, consisting of two steps, the particle streaming step followed by a collision. Rather than other numerical schemes (Haq et al. 2024), the implementation of LBM is relatively straight-forward so that complex boundaries can easily be implemented Guo and Shu (2013). The kinetic nature of the LBM makes it different from other traditional numerical schemes. Its result logic is very simple and can be easily implemented in parallel computing. Bhatnagar et al. (1954) $d_n q_m$ (where n denotes problem given dimension and including the m that denotes the aggregate of individual type directions for streaming density function on regular standard grids) model is used in this section. Flow past two offset cylinders with varying Re and g* by using LBM is not present in literature. Unlike other computational methods, LBM deals with the fluid containing fictive particles and these particles plays a major role in streaming and collision Guo and Shu (2013).

The Boltzmann equation can be explained as follows in the absence of an external force:

$$\partial_t f + \boldsymbol{e}.\nabla f = \psi \tag{2}$$

on f local value not on its surface slope. Collision operators introduce by Bhatnagar et al. (1954) can be written as follows:

$$\psi = \frac{1}{\tau}(f^{(eq)} - f) \tag{3}$$

Here, τ and $f^{(eq)}$ are the relaxation time parameter and equilibrium distribution type function, respectively. Now putting Eq. (3) into Eq. (2) we can get the followings:

$$\partial_t f + \boldsymbol{e}.\nabla f = \frac{1}{\tau}(f^{(eq)} - f) \tag{4}$$

Now the form in term of discretized of Eq. (4) is:

$$\partial_t f_i + \boldsymbol{e}_i.\nabla f_i = \frac{1}{\tau}(f_i^{(eq)} - f_i) \tag{5}$$

By using Chapman-Enskog expansion in Eq. (5) Krüger et al. (2017) we can easily obtain Navier-Stokes equations and Continuity equations. Where streaming and collision part are shown by left- and right-hand side of Eq. (5).

$$f_i(\boldsymbol{x} + \boldsymbol{e}_i.t, t + \Delta t) = f_i(\boldsymbol{x}, t) + \left[f_i^{(eq)}(\boldsymbol{x}, t) - f_i(\boldsymbol{x}, t)\right]\Delta t/\tau \tag{6}$$

The above Eq. (6) is also known as lattice Boltzmann equation and drives the evolution of microscopic mass. The function for the discrete velocity distribution $f_i(\boldsymbol{x}, t)$ and is often referred to as the particle population in LBM. Figure 2. represents the lattice arrangement of *d2q9* model. The presented model is consisted of velocity vectors of number nine. One of the particles is stationary at central node. The we have $f_1, f_2, f_3, f_4, f_5, f_6, f_7,$

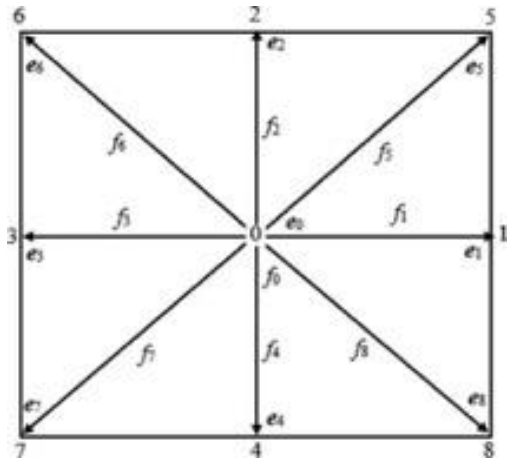

Fig. 2 Lattice structure for d2q9 model

and f_8 are the distribution functions with speed of $\boldsymbol{e}(1,0)$, $\boldsymbol{e}(0,1)$, $\boldsymbol{e}(-1,0)$, $\boldsymbol{e}(0,-1)$, $\boldsymbol{e}(1,1)$, $\boldsymbol{e}(-1,1)$, $\boldsymbol{e}(-1,-1)$, and $\boldsymbol{e}(1,-1)$, where $f_1, f_2, f_3,$ and f_4 move along axis and $f_5, f_6, f_7,$ and f_8 moves alongside with diagonals. Now the weighting factors ξ_i that are $\frac{4}{9}$, $\frac{1}{9}$, $\frac{1}{9}, \frac{1}{9}, \frac{1}{9}, \frac{1}{36}, \frac{1}{36}, \frac{1}{36}$ and $\frac{1}{36}$ for different values of f_0, f_1, f_2, f_3, f_4, f_5, f_6, f_7, and f_8 respectively. The equilibrium distribution function for the lattice Boltzmann method (LBM) is expressed across nine discretized velocity directions as follows:

$$f_i^{(eq)} = \rho\,\xi_i[1 + (2e_i.\boldsymbol{u} - \boldsymbol{u}.\boldsymbol{u})/2c_s^2 + (\boldsymbol{e}_i.\boldsymbol{u})^2/2c_s^4] + o(\boldsymbol{u}^2). \tag{7}$$

Where sound speed is c_s and fluid density is presented by ρ for *d2q9* Wolf-Gladrow (2004). LBM consist of collision and as well as streaming so step for collision is given as:

$$f_i(\boldsymbol{x}, \boldsymbol{y}, t + \Delta t) = f_i(\boldsymbol{x}, \boldsymbol{y}, t)[1 - \xi] + \xi f_i^{(eq)}(\boldsymbol{x}, \boldsymbol{y}, t), \quad i = 0, \ldots, 8 \tag{8}$$

Streaming step can be written as follows:

$$f_i(\boldsymbol{x} + \Delta x, \boldsymbol{y} + \Delta y, t + \Delta t) = f_i(\boldsymbol{x}, \boldsymbol{y}, t + \Delta t), \quad i = 1, \ldots, 8 \tag{9}$$

Here Δx and as well as the Δy indicates the lattice spacings both in the stream wise as well as transverse direction, respectively. In term of summation of distribution function, the macroscopic type of fluid density in each lattice is given as:

$$\rho = \sum f_i, = \sum f_i^{(eq)}, \quad i = 0, \ldots 8. \tag{10}$$

The macroscopic kind of velocity can be written as:

$$\rho\boldsymbol{u} = \sum e_i f_i, = \sum e_i f_i^{(eq)} \quad i = 0, \ldots 8 \tag{11}$$

By using equation of state, we can calculate pressure as:

$$p = \rho c_s^2. \tag{12}$$

The single based relaxation depending on the time parameter is intricately connected to the viscosity of a fluid, and it is expressed as follows:

$$v = \Delta x^2 c_s^2(\tau - 0.5)/\Delta t. \tag{13}$$

Table 1 Independence grid analysis (D) around a square cylinder with a Reynolds number of 150

D	C_{Dmean}	St	C_{Drms}	C_{Lrms}
10.0	1.6005(5.85%)	0.1728(4.29%)	0.0825(6.1%)	0.2918(5.6%)
20.0	1.5060	0.1634	0.00274	0.2649
30.0	1.5394(5.8%)	0.1622(0.85)	0.0272(1.01%)	0.1738(0.75%)

Table 2 Upstream location $\frac{Lu}{D}$ influence for Reynolds number of 150 on the airflow around a square cylinder

$\frac{Lu}{D}$	C_{Dmean}	St	C_{Drms}	C_{Lrms}
5.0	1.660(2.91%)	0.1586(2.45%)	0.0279(2.45%)	0.2919(2.52%)
10.0	1.5260	0.1744	0.00274	0.2849
15.0	1.5338(1.10%)	0.1732(0.75%)	0.0162(1.15%)	0.2741(0.75%)

Table 3 Downstream location $\frac{Ld}{D}$ influence for Reynolds number of 150 on the airflow around a square cylinder

$\frac{Ld}{D}$	C_{Dmean}	St	C_{Drms}	C_{Lrms}
25.0	1.5502(1.45%)	0.1682(1.75%)	0.0167(1.67%)	0.2694(1.65%)
35.0	1.5260	0.1744	0.00274	0.1749
55.0	1.5362(0.68%)	0.1644(0.71%)	0.0271(0.69%)	0.1732(0.7%)

2.3 Initial Conditions

The provided simulations of every possible case selected in this study that were initially started along with a stationary fluid where the velocity (u = v = 0), with the exception of for the nodes at the edges.

2.4 Boundary Conditions

At the inlet position, the source boundary conditions mean inflow are given as:

$$u = U_{\infty,} \text{ and. } \quad v = 0, \tag{14}$$

At the domain's exit, the convective boundary condition [49] is used.

$$\partial_t u_i + u_{conv} \partial_x u_i = 0 \tag{15}$$

u_{conv} was set toward the uniform type of inflow kind of velocity in Eq. 15 and at outflow u_{conv} cannot be zero it must be positive. Depending on the problem, u_i can be a function of temperature, pressure, or velocity in a convective boundary condition. On the other hand, no-slip boundary conditions are imposed to the main cylinders body surfaces and the bottom and upper walls of the computing domain have periodic boundary conditions (Guo and Shu 2013).

3. GRID-INDEPENDENCE AND VALIDATION OF CODE

Before presenting the main findings from the numerical simulations, this section addresses the issues of independence for grid, independence of domain, and validation for code. Table 1 displays the result of the grid-independence test for the mean drag coefficient (C_{Dmean}) C_{Drms}, C_{Lrms}, and St. All values in table 1, 2, 3 are calculated using Eq. (16).

$$proportion\ of\ inaccuracy = absolute\ value\ (Greatest\ value - Smallest\ value)/ Greatest\ value) * 100 \tag{16}$$

The scale of the computational type set of a domain in all across the three cases chosen cases ($D = 10.0, 20.0\ and\ 30.0$) is same [i.e.,$L_U/D = 10.0$, $L_d/D = 35.0$ and with impediment percentage $L_y/D = 5.0$].

4. CALCULATION

In current section, we have discussed characteristics of flow behind offset square cylinder using important parameters *Re* and g* from 1 to 150 and 0.5 to 5. We will also discuss different flow features and force characteristics for flow behind square cylinders. The most imported computed results will be presented to prevent repetition. The visualization of instantaneous vorticity contour for fixed value of $g^*= 1$ and varying Re is presented in Figs. 3(a-e). At $Re = 1$, fully steady flow is observed in whole computational domain, and the flow is generated by the cylinders with respect to wake center lines which is resulting in the generation of symmetric bubbles and is referred to as steady attached flow (Fig. 3(a)). Figure 3(b) also shows steady flow with increasing recirculation bubbles length due to increment in Re. Separation in steady flow regimes can manifest from both the top and as well as bottom sides of cylinders. Now in Fig. 3(c) it can be clearly seen that wake is no longer steady and onset of vertex shedding begun with weaker vortices and longer wake region can be observed as compared to the Figs. 3(a, b). The Serpentine nature of the C_2 and two minor vortices that near the exit demonstrate the wide wing of the distance like a streamwise for the vortices and is known as wide-wake flow regimes for shear layer reattachment. At $Re = 150$ generation of vortices started from both cylinders at downstream position which is like the Meneghini et al. (2001) findings

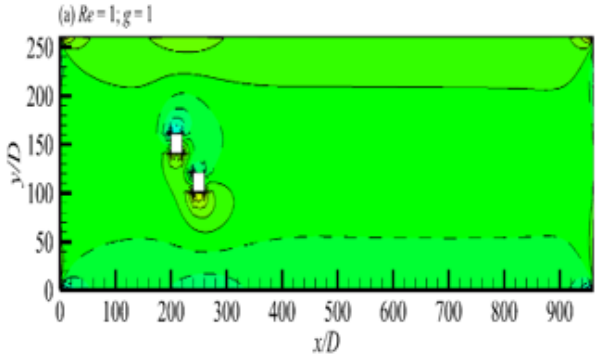

(a) For Re= 1.0 and at fixed g^*= 1.0

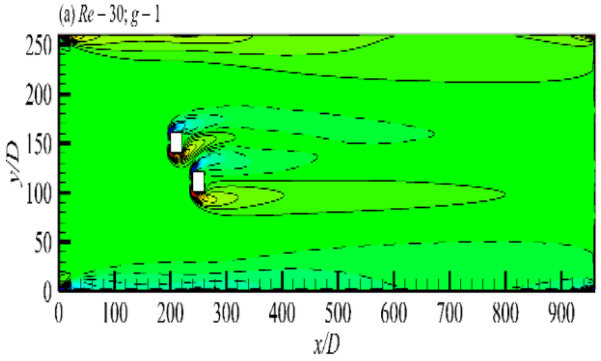

(b) For Re= 30.0 and at fixed g^*= 1.0

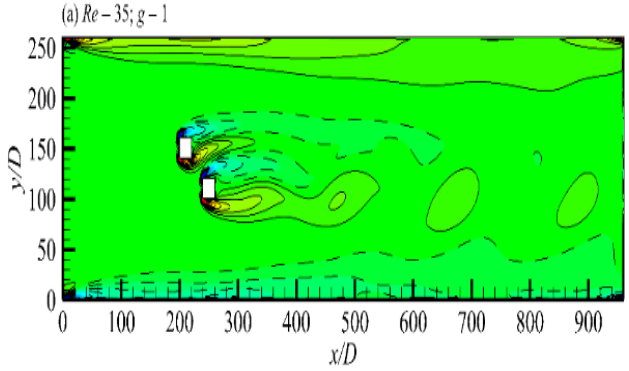

(c) For Re= 35.0 and at fixed g^*= 1.0

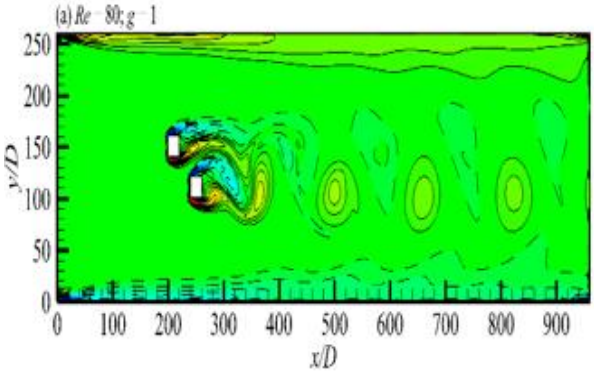

(d) For Re= 80.0 and at fixed g^*= 1.0

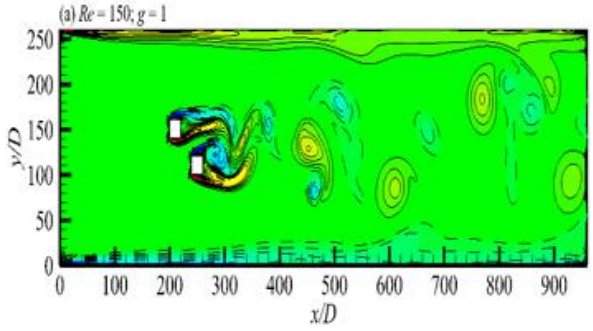

(e) For Re= 150.0 and at fixed g^*= 1.0

Fig. 3 Vorticity contour type visualization of flow past two offset squared cylinders at various *Re* and at fixed g^*

Table 4 The influence of blockage ratio β on the flow surrounding a square-shaped cylinder with Reynolds number of 150

β	C_{Dmean}	St	C_{Drms}	C_{Lrms}
8.0	1.6562(2.6%)	0.1582(2.3%)	0.01691(2.8%)	0.2915(2.3%)
13.0	1.5262	0.1545	0.00275	0.2848
18.0	1.5325(1.1%)	0.16381(1.0%)	0.0271(1.1%)	0.2821(0.9%)

for $g^* \leq 3$ (Fig. 3(d)). Moreover, with increasing Re the irregular and non-periodic behavior is observed behind both cylinders and can be referred to flipflopping flow pattern (Fig. 3(e)).

As shown in the vorticity graphs above, flow characteristics evolve from steady to unstable, followed by the production of periodic vortices and finally from periodic to totally irregular and complicated flow. The same pattern can be seen in Figs. 4(a-d). In a time history analyzation of C_D and C_L, a straight line is observed at $Re = 1$ and 30, which signifies that flow is stable and there are no transverse oscillations in the wake for these Re, with further incrementation in Re flow shows sinusoidal behavior with amplitude difference for C_{D1} and periodic behavior with amplitude difference is noticed for C_{D2} ($Re = 35$ and 80), and at $Re = 150$ drastically unsteady and non-periodic flow can be observed which shows irregular variation with time and such type of flow can be recommended to flip-flopping type of flow pattern (Fig. 4(a, b)). In Figs. 4(c, d) steady behavior with no transverse oscillation is observed at $Re = 1$ and 30, quasi unsteady behavior is observed for C_{L1} and periodic behavior can be noticed for C_{L2} at $Re = 35$. At $Re = 180$ periodic behavior with amplitude difference can be noticed for both C_{L1} and C_{L2}, whereas unsteady and non-periodic flow behavior is noticed for C_L at $Re = 150$

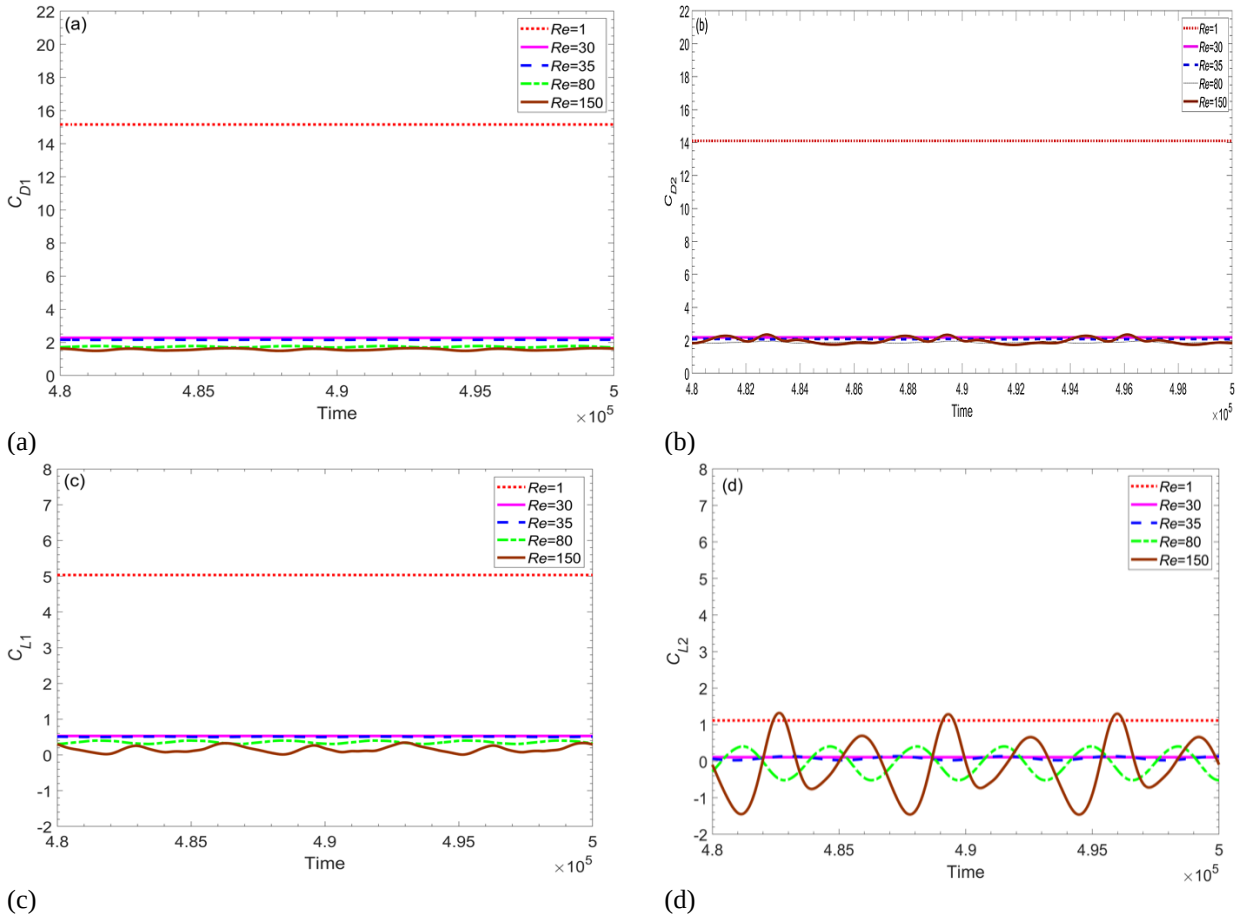

Fig. 4 Result for analyzing the temporal evolution of forces under varying conditions with Re and fixed $g^*= 1.0$

The power type spectrum analysis of C_L at various values of Re, and fixed $g^*= 1$ is displayed in Figs. 5(a-d). The first primary vortex shedding frequency are represented by the largest peak in the graphs, and the frequencies for secondary cylinder type interaction are presented by other peaks. No peak is observed at $Re = 1$ and 30 and for St_1 of $Re = 35$ that's why these graphs are not included. At $Re = 35$ One primary vortex shedding frequency is observed at St_2 indicating that vortex formation has started behind downstream cylinder (Fig. 5(a)). One little peak can be seen at $Re = 80$ on St_1 graph in Fig. 5(b), and one large peak can be observed at Fig. 5(c). Secondary peaks with the principal vortex shedding exist at $Re = 150$, confirming the impact of secondary kind of cylinder interaction frequencies that is on flow features, particularly vortex shedding of the cylinders at the St_2 and similar behavior with smaller amplitude is noticed for St_1which is not shown (Fig. 5(d)). Furthermore, it's important to acknowledge that when Re increases, the primary peak for both cylinders increase as well, and we also found different numerical values for C_1 and C_2 of St.

Now Figs 6(a-d) as well as the Figs 6(a-d) show the vorticity contour show visualization for entirely distinct g^* from 0.5 to 5 at fixe $Re = 150$. These graphs clearly illustrate the influence of value of g^* on characteristics of flow. We can observe from graphs that at $g^*= 0.5$ jet flow merge within the shed style of vortices at down-stream position of the given cylinders which results in a regular shed vortex with different wake length (Fig. 6(a)). In Fig. 6(b) with the passage of time shed vortices change its behavior continuously, and in far-wake region one can clearly observe unsteadiness in flow behavior and such type of flow pattern can be named as flipflopping flow pattern, because as they go downstream, shed vortices interact intensely with each other forming a trend. At $Re = 150$ and $g^*= 3$ it is clearly illustrated the in-phase separation behind both cylinders and it can be clearly seen that provides the negative type vortices are generating from upper side corner of C_1 and C_2 and lapse is investigates among the vortex of type of shedding due to existence of both type streamwise and transverse distance intervals among cylinders due to which irregularities can be watchable at far downstream of the cylinders (Fig. 6(c)). Due to large g^* the wake between offset cylinders have practically dissipated and we saw periodic separation of vortices from both cylinders in alternate pattern, which creating oscillating type wake in the form of two distinct vortices (Fig. 6(d)).

Figures 7(a-d) represents the analysis of time-based account of both type C_D as well as C_L. The flow is unsteady and unpredictable, and it varies irregularly throughout time at $g^*= 0.5$, also it can be seen that size and as well as the length of shed vortices change uniformly, such type of low pattern is an example of bistable flow that shows the pattern. At $g^*= 1.5$ and 3 the presence of modulated C_D signal is noticed with amplitude difference which is due to fact that size and shape of the vortices is not same for both

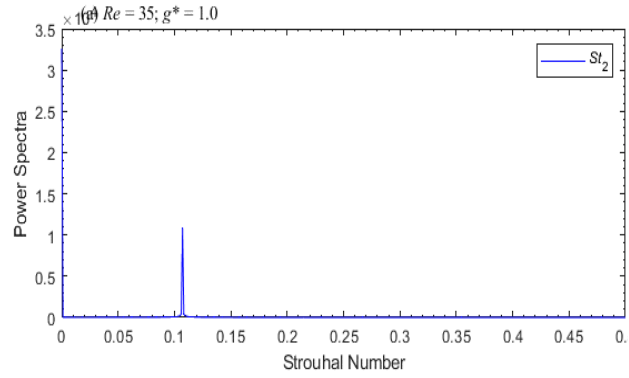

(a) $Re = 35$ and fixed $g^*= 1$ of lift coefficients

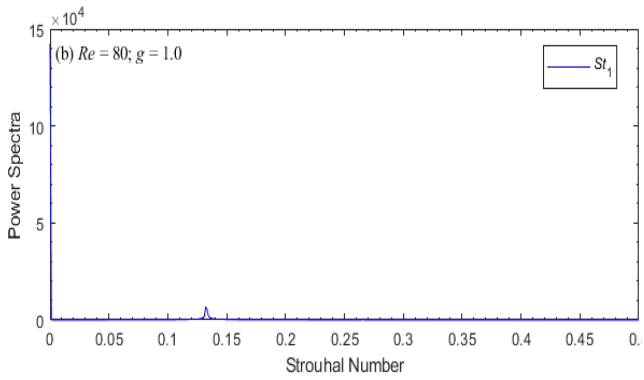

(b) $Re = 80$ and fixed $g^*= 1$ of lift coefficients

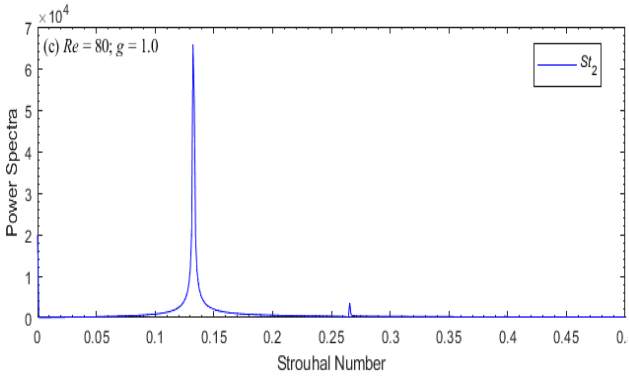

(c) $Re = 80$ and fixed $g^*= 1$ of lift coefficients

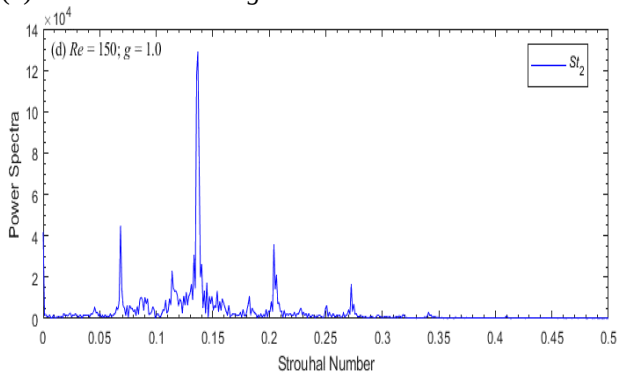

(d) $Re = 80$ and fixed $g^*= 1$ of lift coefficients

Fig. 5 Analyzing the power spectra at various values of Re and fixed $g^*= 1$ of lift coefficients

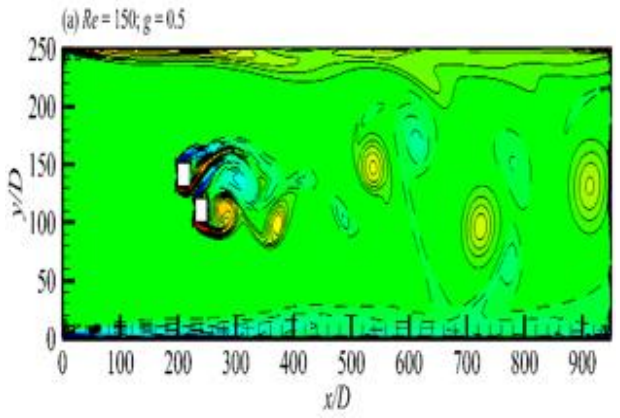

(a) For $g^* = 0.5$ and at fixed $Re = 150$

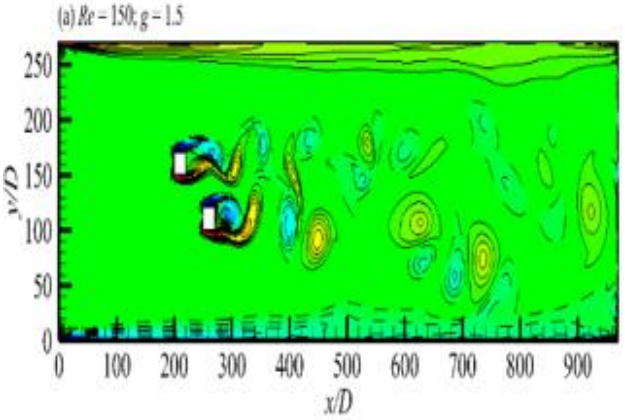

(b) For $g^* = 1.5$ and at fixed $Re = 150$

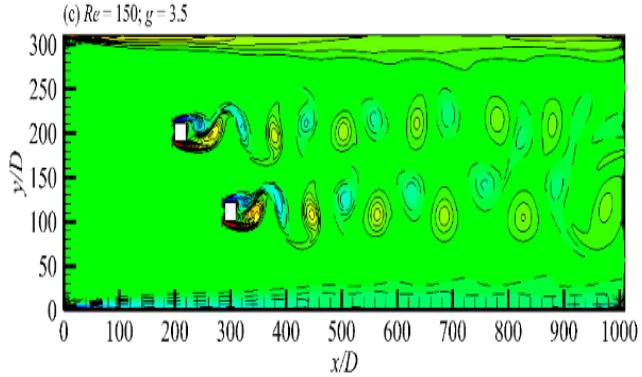

(c) For $g^* = 3.5$ and at fixed $Re = 150$

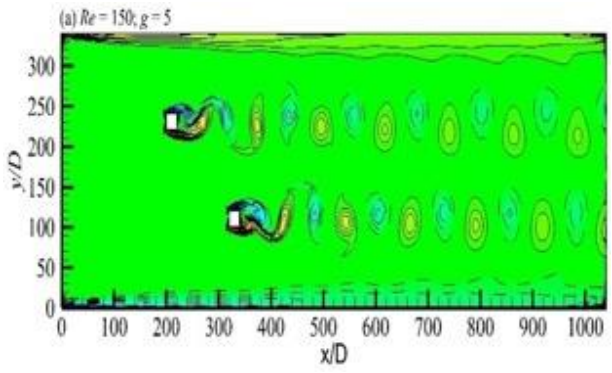

(d) For $g^* = 5.0$ and at fixed $Re = 150$

Fig. 6 Visualization of vorticity contours in the flow around two square cylinders positioned off-center, with variations in their configuration of g^* and at fixed $Re = 150$

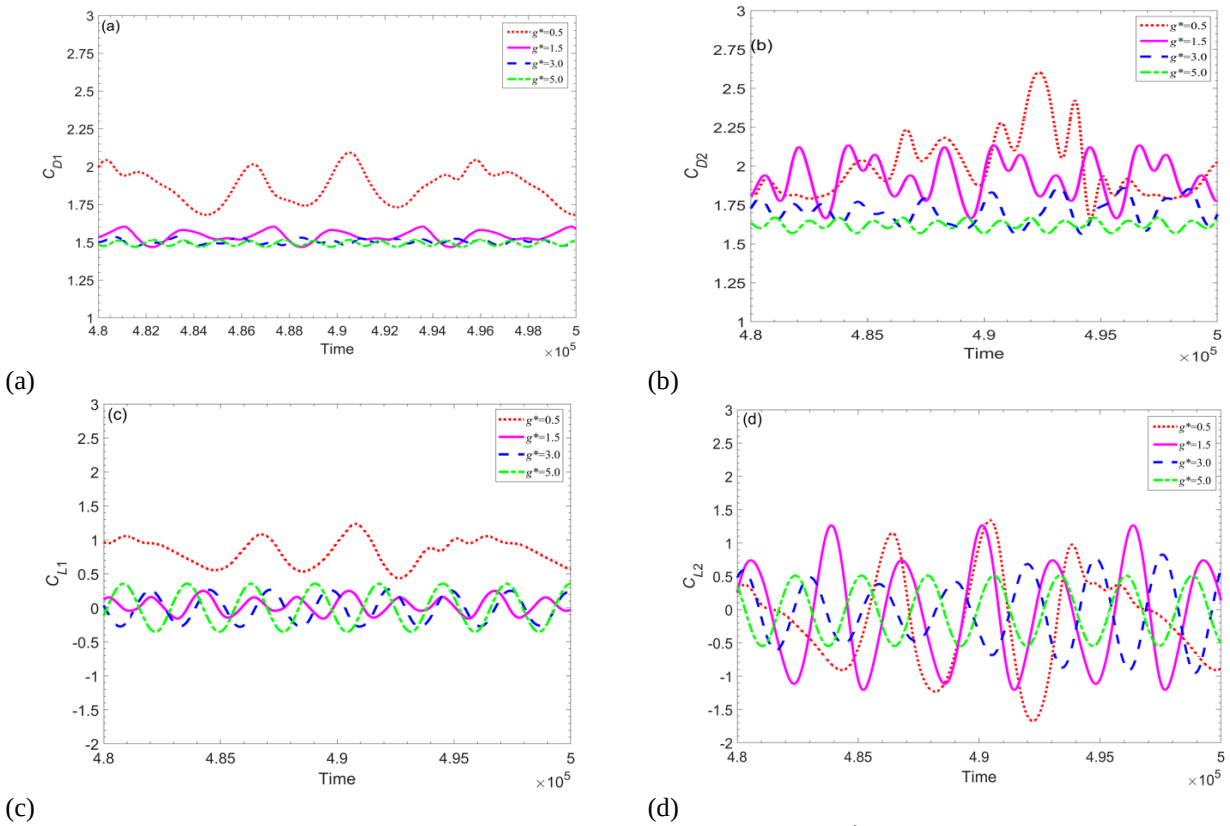

Fig. 7 Time history investigation and analysis of forces at varying g^* and at fixed $Re = 150$

cylinders. Whereas at $g^* = 5$, we can see that periodic behavior behind both cylinders, where C_2 experience higher C_D than the C_1 and both cylinders behave like single cylinder with periodic fluctuations (Figs. 7(a, b)). On the other hand, in C_L shows similarity with C_D at $g^* = 0.5$. At $g^* = 1.5$ and 3 periodic nature with fluctuations is observed for both C_{L1} and C_{L2} which indicate that amplitude is increasing for period of sometime before declining with each subsequent cycle and at $g^* = 5$, C_L exhibits sinusoidal behavior due to alternate vortex shedding from the cylinder, confirming antiphase synchronized vortex shedding with periodic fluctuations (Figs. 7(c, d)).

Figure 8 (a-f) shows the power spectrum type of analysis of C_L at different $g^* = 0.5$ to 5 and at fixed Re. Multiple irregular scattering frequencies are observed with the pre-dominant primary vortex frequency. The vortices are affected by the jet flow, resulting in the presence of several peaks due to highly modulated C_L signals, and we can also see that St of C_2 is more affected than C_1 (Figs. 8 (a-e)). For both cylinders, the major vortex shedding frequency is only visible at $g^* = 5$ at St_2 (Fig. 8(f)). At $g^* = 1.5$ and 5 St_1 graphs are not included because of similar behavior with St_2. Primary vortex shedding frequency is the highest peak in the spectrum and it is also worth noting that with increasing in space between cylinders reduces irregularities in flow.

Figures 9 (a-d) describes vorticity contour at fixed $g^* = 2.5$ and varying Re. At $Re = 35$ steady flow is observed throughout the domain computational model with no transition. In Fig. 9(a), the flow is constant, and as well as the separation take place on both the top as well as the bottom sides of the C_1, and immediately reattaches itself to the C_2 such a flow regime is known as steady flow regime. We can also observe that the wavelength increases with increasing the Re. In Fig. 9(b) it can be clearly seen that wake is no longer steady and onset of vertex shedding begin with weaker vortices, which can be seen in far downstream position. At $Re = 75$ we can observe in-phase flow separation behind both cylinders and negative side of vortices are generating from upper side of both upstream and downstream cylinders. The wake behind both cylinders is narrow and wide, and no relationship can be found between them because moving toward downstream position they flipped from one to another and can be referred to flip-flopping flow regime (Fig. 9(c)). The antiphase combination occurs at $Re = 125$. Flow shows approximately periodic behavior up to sometime but at far downstream position wake becomes complexed and shows merging behavior (Fig. 9(d)).

Now again the analysis of time history of both C_D and C_L at fixed $g^* = 2.5$ and with varying Re is presented in Fig. 10(a-d). The C_D of both type of cylinders are constant at $Re = 35$. This is because the shear layers that are emerging from the side of C_1 neither reattach to C_2 nor roll up to due to vortices in the gaps with further increment at $Re = 40$ the C_D of both cylinders shows a little fluctuation which is the indication of switching to wake mode. The C_D at $Re = 75$ and 125 fluctuate and are bistable which is a sign of the presence of the modulated C_D signals this behavior is because size and shape and the magnitude of modulation is not same for both cylinders (Fig. 10(a, b)).

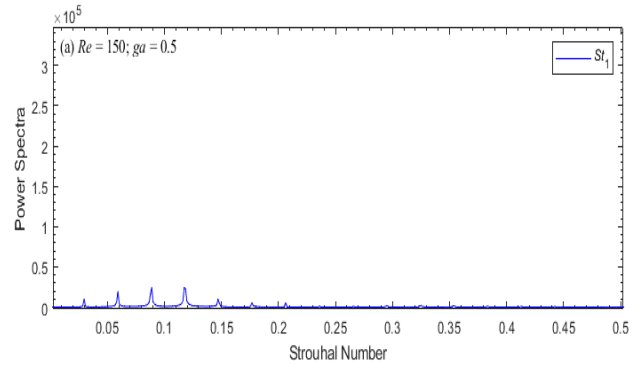

(a) For $g^*= 0.5$ of lift coefficients and fixed Re

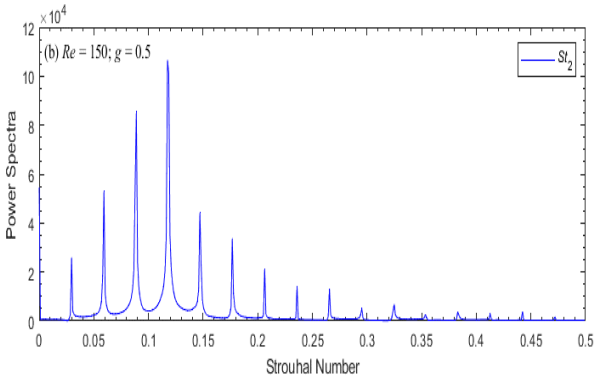

(b) For $g^*= 0.5$ of lift coefficients and fixed Re

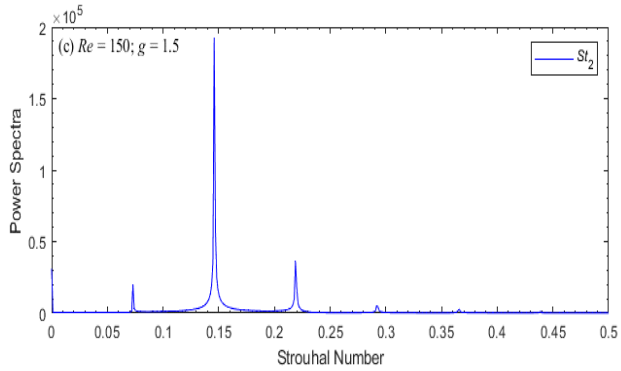

(c) For $g^*= 1.5$ of lift coefficients and fixed Re

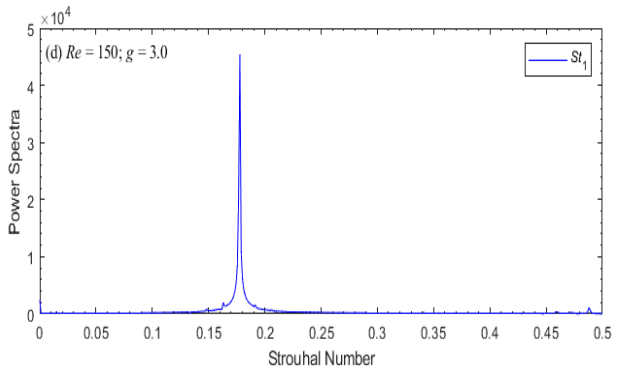

(d) For $g^*= 3.0$ of lift coefficients and fixed Re

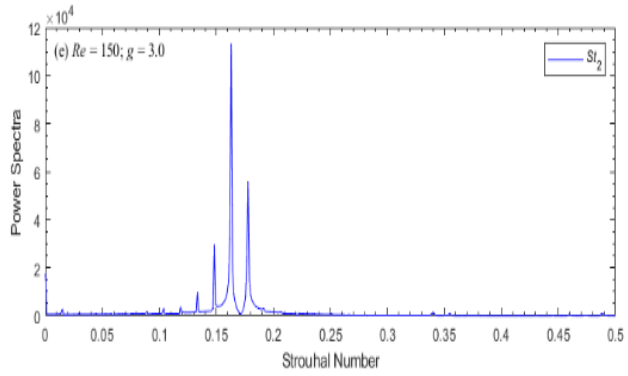

(e) For $g^*= 3.5$ of lift coefficients and fixed Re

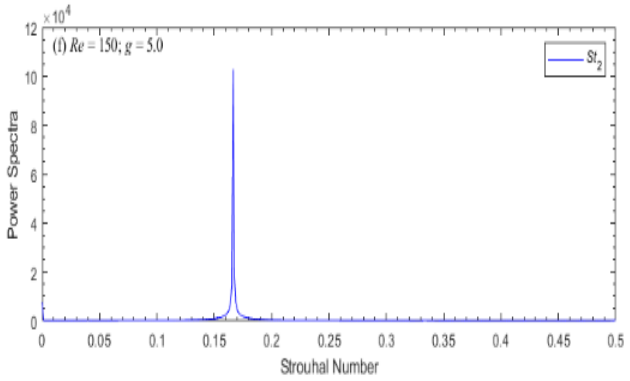

(f) For $g^*= 5.0$ of lift coefficients and fixed Re

Fig. 8 Power spectra analysis of coefficients lift at varying g^* and at fixed $Re = 150$

Whereas C_L plots shows steady behavior with no fluctuation at $Re = 35$, and at $Re = 40$ the C_L of both cylinders have periodic behavior with large difference in their magnitude, C_{L1} magnitude is smaller than C_{L2}, and magnitude of the fluctuation of C_{L1} is almost disappeared and at $Re = 75$ and 125 the amplitude of the consecutive cycle of C_{L2} is unpredictable and irregular because it shows increasing and decreasing behavior with respect to time. C_{L2} curve is bistable due to quasi-steady state condition of flow and C_{L1} curve is periodic with the same amplitude at (Fig. 10(c, d))

From the Fig.s 11(a-d) that depicts a power spectrum study of C_L at fixed $g^* = 2.5$ and for various Re. The C_1 plot at $Re = 40$ is excluded because of steady behavior and only one shedding frequency of primary vortex is observed for C_2 which indicate that vortex generation starts behind C_2 (Fig. 11(a)). we can observe secondary peaks with shedding frequency of primary vortex as Re increases confirming the impact of the secondary type cylinder with a frequency of interaction with the flow and particularly on the vortex side of shedding of the cylinders and at $Re = 75$, St_1 graph shows similarity with St_2 and is not shown (Fig. 11(b-d)). As a comparison to C_1, C_2 shows more disturbed frequencies for St and irregularities in frequency increases as Re increases.

Figures 12(a-e) shows instantaneous contour visualization for fixed $Re = 100$ at different g*. At g* = 1.0 (Fig. 12(a)), we found alternate shed vortex behind C_1 with only a minor interaction with C_2. This flow regime is likewise referred to as weakly interactive vortex shedding flow regime and is known is flip-flopping wake pattern. Due to small g* vortices are not clearly visible near and far downstream position and compared to regular vortices, some of these are narrower. This shows that between the cylinders gap there exists a strong interaction of flow and can be named as synchronized flow in near downstream

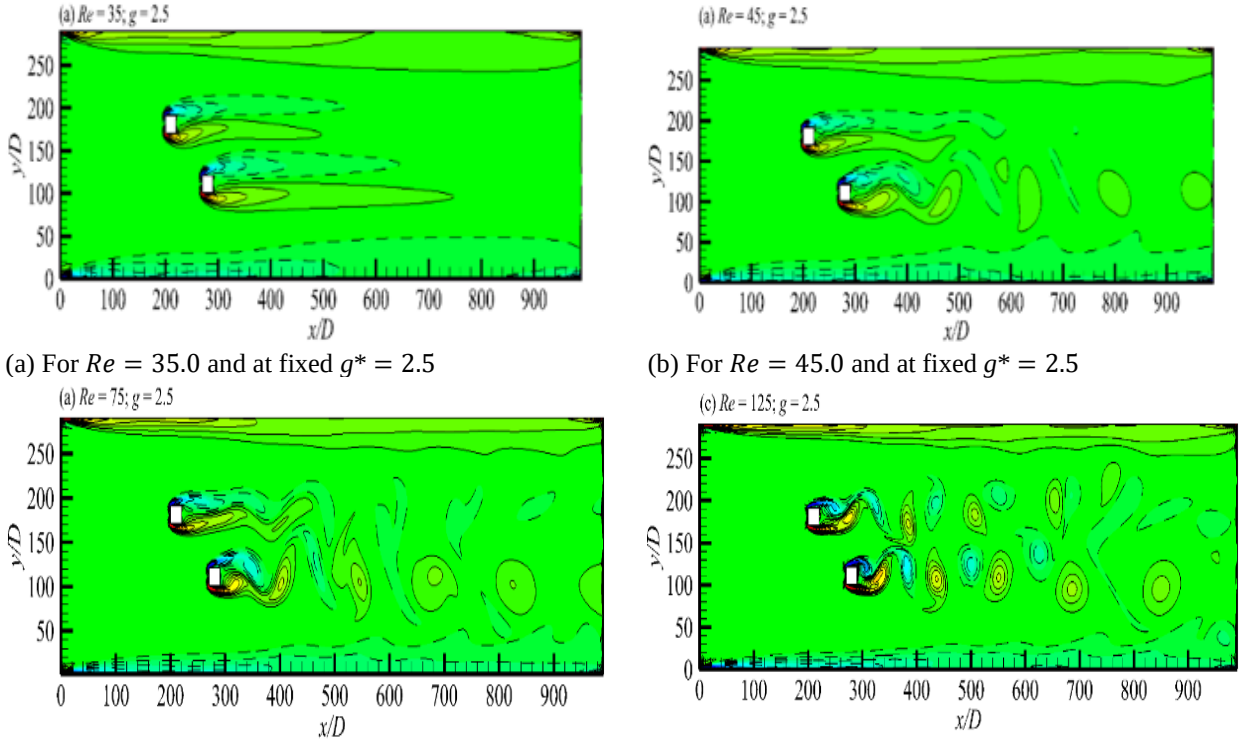

(a) For $Re = 35.0$ and at fixed $g^* = 2.5$

(b) For $Re = 45.0$ and at fixed $g^* = 2.5$

(c) For $Re = 75.0$ and at fixed $g^* = 2.5$

(d) For $Re = 125.0$ and at fixed $g^* = 2.5$

Fig. 9 Visualization of vorticity contour of flow past two offset square cylinders at different Re and at fixed $g^* = 2.5$

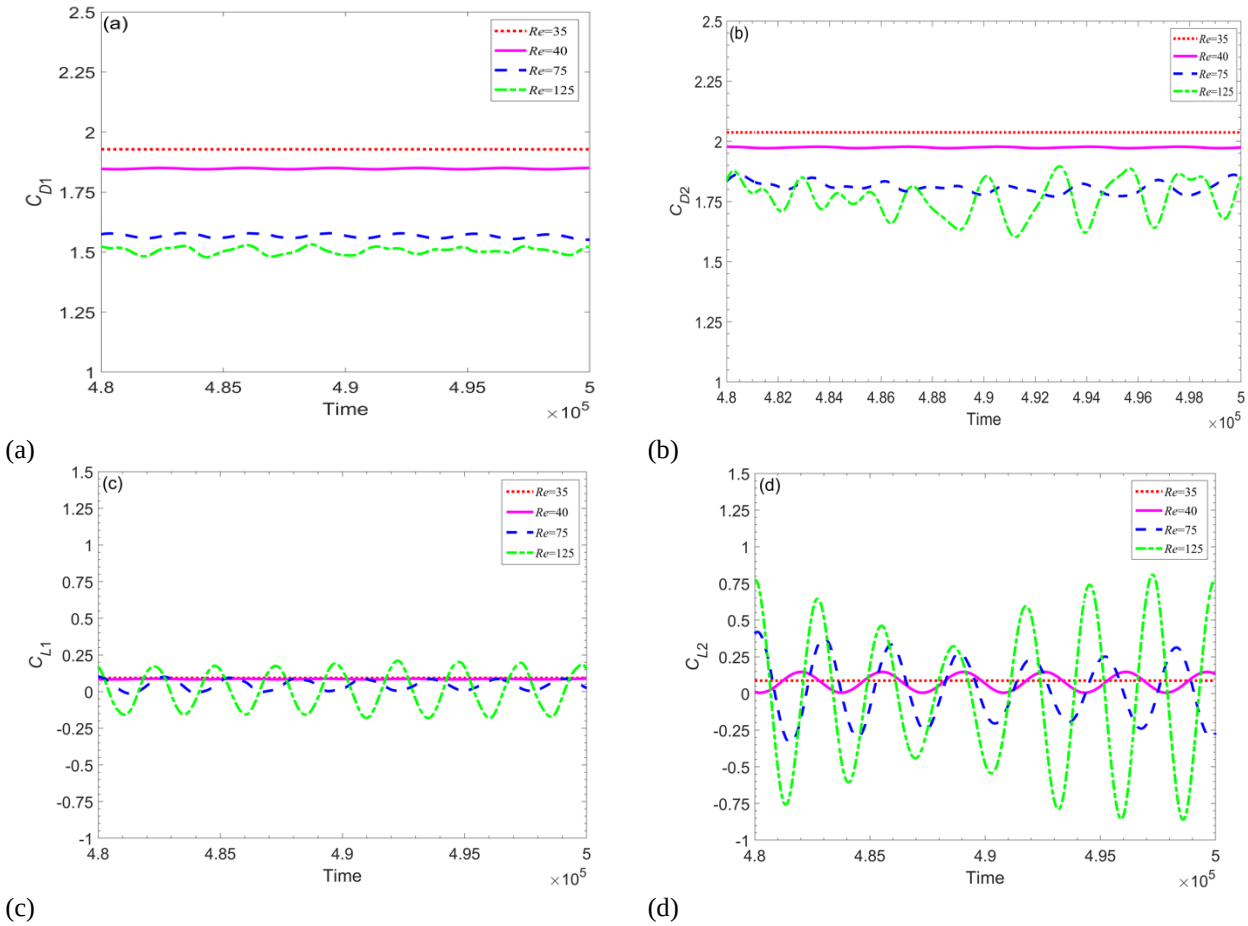

(a)

(b)

(c)

(d)

Fig. 10 Time history investigation and analysis for forces at various values of Re and at fixed $g^* = 2.5$

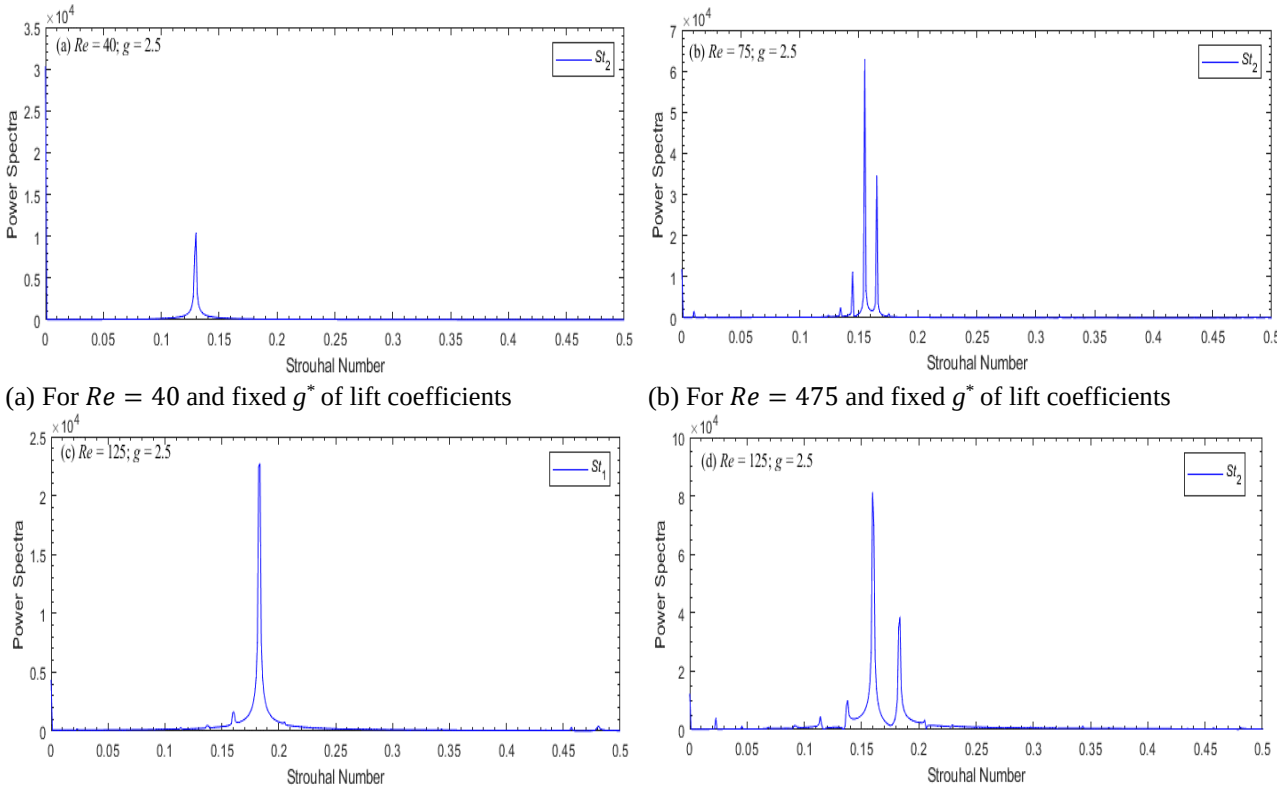

(a) For $Re = 40$ and fixed g^* of lift coefficients

(b) For $Re = 475$ and fixed g^* of lift coefficients

(c) For $Re = 125$ and fixed g^* of lift coefficients

(d) For $Re = 125$ and fixed g^* of lift coefficients

Fig. 11 Power type spectra analysis at different value for Re and fixed g*= 2. 5 of lift coefficients

position (Fig. 12(b)). At g* = 4.0, vortices are generated in same phase from both cylinders and are periodic. We can observe that in both cases flow roll up quickly and form vortices, and in near wake region vortices are in development stage and such type of wake pattern can be known as non-synchronized wake pattern and can be referred to as Von-Karman vortex street Fig. 12(c)).

Whereas at g∗= 1 due to the vortex shedding both C_D exhibit periodic behavior in time history analysis with different amplitude and consecutive cycles. This is due to the fact that when Re grows, as the inertial forces increase, and the stronger the viscous forces are in relation to the oscillation's magnitude C_D and C_L increases; in both scenarios, the amplitude of C_2 is greater than. At g*= 2 and 4, in the C_2 wake there is Since there is sufficient room for the vortices to roll up, the amplitude of C_2 is larger than C_1 as we can observe and C_D shows a modulated signal with a difference in amplitude between both cylinders and modulation is because of the size and shape of the vortices (Fig. 13(a, b)). Furthermore, at g*=1 C_L graphs show periodic kind of behavior with different amplitude and at g*=2 the flow of C_1 curves of both cylinders have a periodic nature due to quasi-unsteady condition with the amplitude of consecutive cycles fluctuating with time. Whereas, due to the alternate type shedding of different vortices from the shape of square cylinders, the time-history that shows study of both cylinders as a sinusoidal behavior and the duration of the C_{L2} signals are twice as compared to the C_{L1} at g*=4 (Fig. 13(c, d)).

The power spectrum analysis of C_L for the fixed $Re = 100$ with varying g* from 1 to 4 with 1 increment is presented in Figs. 14(a-d). At g*= 1.0, C_1 has one little peak of St, while C_2 has minor secondary peaks that shoes behavior with primary vortex shedding frequency of St (Fig. 14(a, b)). At g*= 2 multiple and irregular scattered frequencies can be observed, and these peaks are because of modulated C_1 signals. The graph of C_1 signals also demonstrate that the C_2 is severely affected and one dominant peak is observed at g*= 4 which indicate that there is no distortion (Figs. 14(c, d)). St graphs of C_1 at g*= 2 and 4 because these graphs exhibit same behavior with C_2. We can see from these power spectrum graphs that flow is completely established at large g* and is scattered and irregular for small g*.

The variations in C_Dmean values across a range of 'g*' values from 0.5 to 5 and Reynolds numbers (Re) spanning from 1 to 150 are shown in Fig.s 15(a-e). Notably, both types of cylinders have very high C_Dmean values at Re = 1, which drastically decline as Re rises to 5. The growing impact of inertial forces is the cause of this behavior. Up until Re = 55, the trend shows a declining pattern before constant and nearly steady flow conditions are noticed. This is principally caused by the viscous forces' diminishing effects as Re rises, which leads to a thinner shear layer and less drag forces. Additionally, a consistent behavior is seen from Re = 60 onwards up to Re = 150, indicating an unsteady flow state. Notably, C_Dmean2 for both varieties of cylinders is marginally greater than C_Dmean1 and along with the lone cylinder. This disparity is explained by the fact that C_2 is unshielded whereas C_1 is protected by C_2, which causes C_2 to be subjected to stronger forces than C_1. In addition, compared to transitional and unstable flow

situations, steady-state flow is observed to have C_Dmean at its highest value. There is a slight difference in C_Dmean values when 'g*' values are less, but when 'g*' values rise, this difference disappears. For instance, variations in C_Dmean values are apparent in Fig. 15(a) at 'g*' = 0.5 and 1, whereas in Fig. 15(e) at 'g*' = 4.5 and 5, these differences are practically imperceptible, and the C_Dmean values for SC, C_1, and C_2 closely align, seeming like a single line.

Figure 16(a-e) shows root mean square values at varying g^* and Re from 0.5 to 5 and 1 to 150. It can be observed from Fig. 16(a) that up $Re = 30$ all cylinders show constant behavior. Re =35 shows increasing behavior with increment in Re and this change in trend is related to a shift in the flow state. It is evident that between $Re = 65$ and 80 the values of C_{Drms} at $g^* = 1$ are less than SC. Except at these aforementioned Re the C_{Drms} values of both cylinders are higher as compared to SC. Further, up to $Re = 125$ the values of C_{Drms1} and C_{Drms2} at $g^* = 0.5$ are higher than values $g^* = 1$ and from $Re \geq 135$ we can see those values of C_{Drms2} at $g^* = 1$ is increasing from C_{Drms1} at $g^* = 0.5$ and it can be predicted that with increasing the values of Re the values of C_{Drms2} are greater as compared to C_{Drms1}. The values of C_{Drms} of both cylinders at $g^* = 1.5$ and 2 are presented in Fig. 16(b). Constant behavior is observed till $Re = 35$ and after that increasing trend can be seen with increment in Re for both cylinders. Sudden jump is observed for C_{Drms2} at $g^* = 2$ when it advances over $Re = 180$. Overall, C_{Drms2} values are a lot more than that of C_{Drms1} it suggests that more drag force is exerted on C_2. From $Re = 55$ to $Re = 80$ one can notice that values of SC increase and have highest values, after that decreases for some time. From $Re = 110$ to onwards C_{Drms} values of both

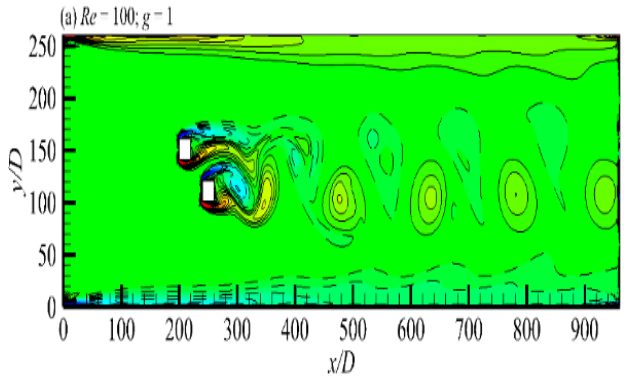

(a) Vorticity Contour at $g^* = 1.0$ at fixed Re

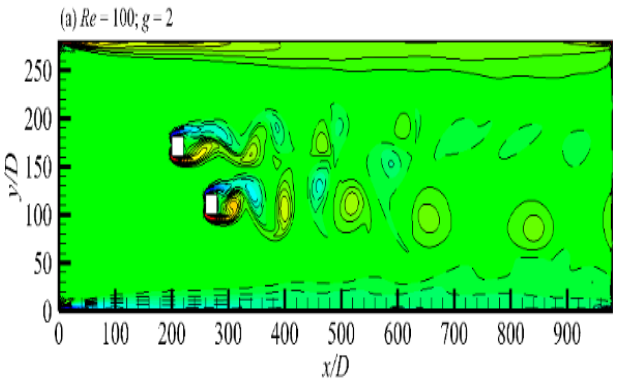

(b) Vorticity Contour at $g^* = 2.0$ at fixed Re

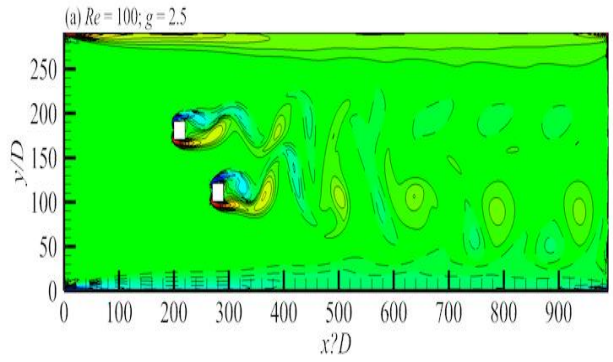

(c) Vorticity Contour at $g^* = 2.5$ at fixed Re

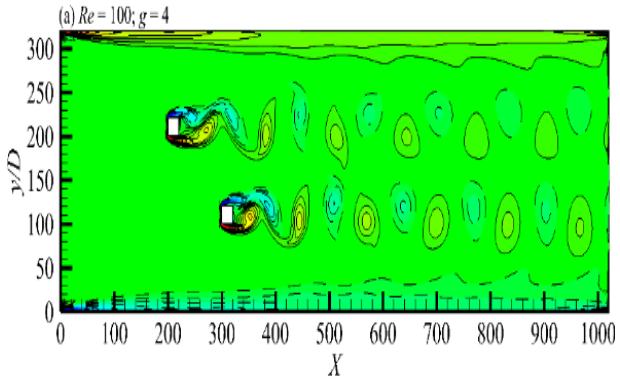

(d) Vorticity Contour at $g^* = 4.0$ at fixed Re

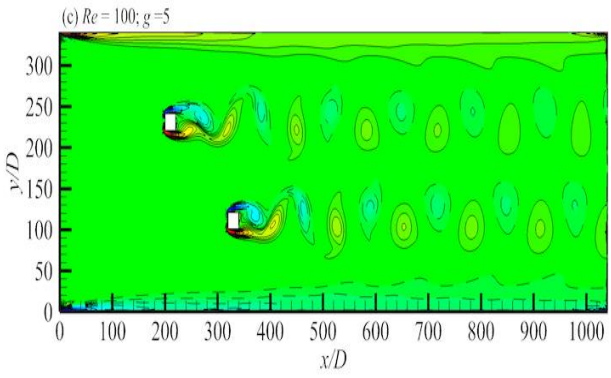

(e) Vorticity Contour at $g^* = 5.0$ at fixed Re

Fig. 12 Vorticity Contour visualization of flow past two offset square cylinders at different g^* at fixed $Re = 100$

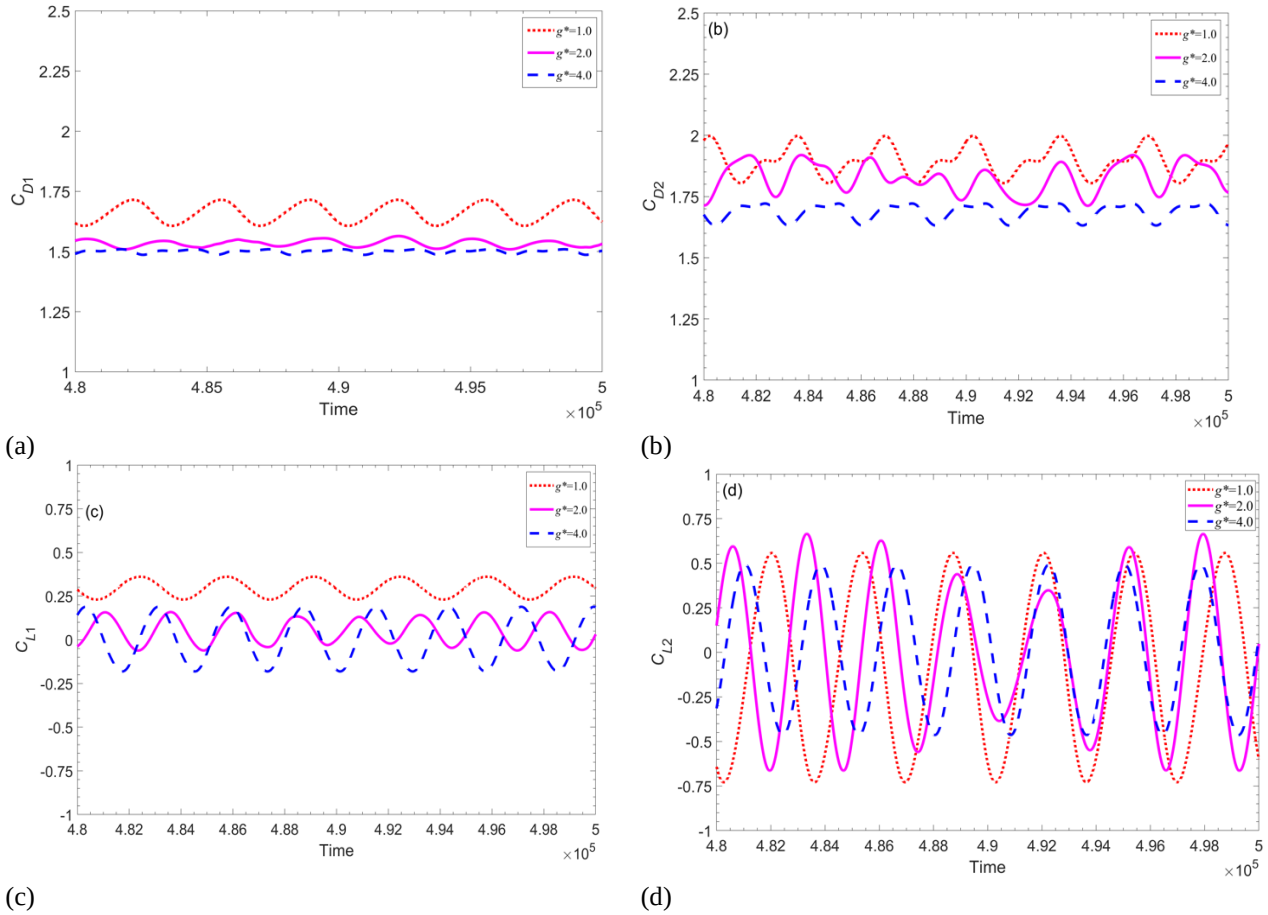

Fig. 13 Time history investigation and analysis for forces at various values of g* and for forces at fixed $Re = 100$

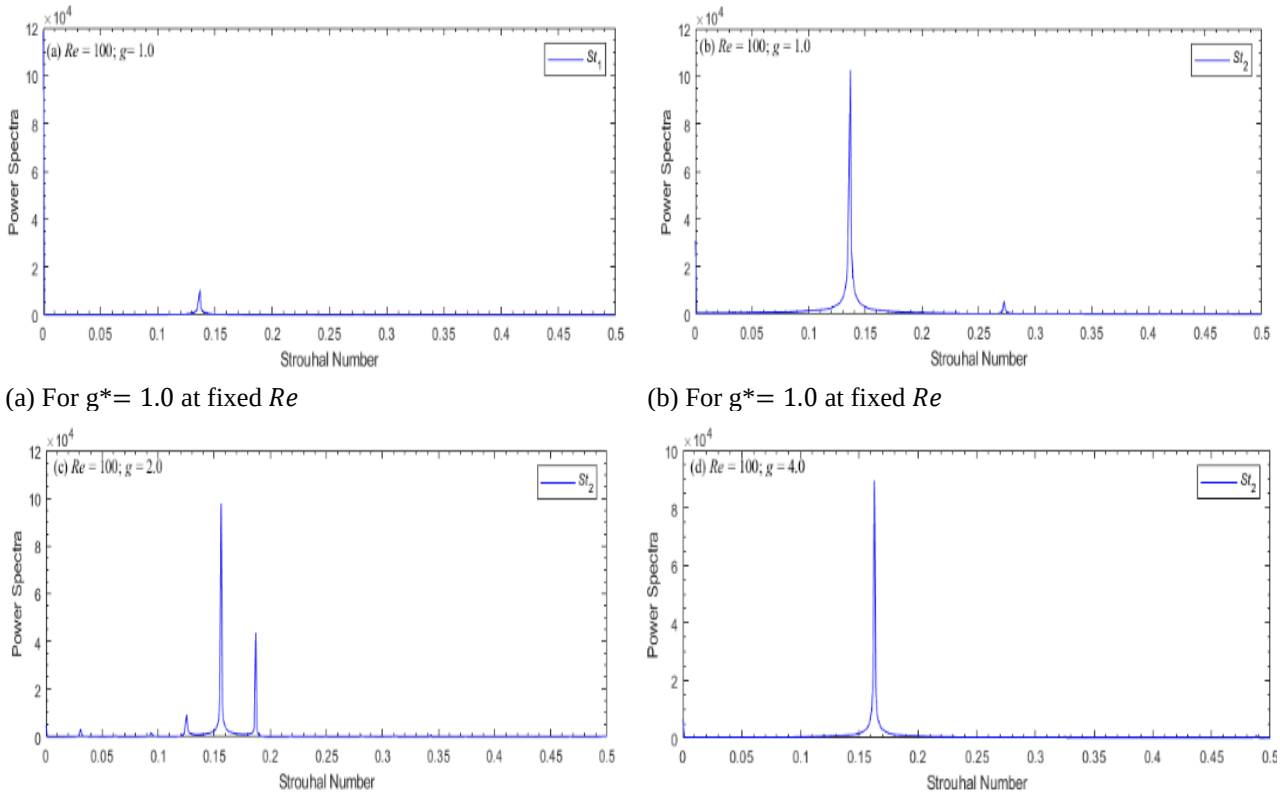

(a) For g*= 1.0 at fixed Re (b) For g*= 1.0 at fixed Re

(c) For g*= 2.0 at fixed Re (d) For g*= 4.0 at fixed Re

Fig. 14 Examination of power spectra and lift coefficient studies at various g* at a fixed $Re = 100$

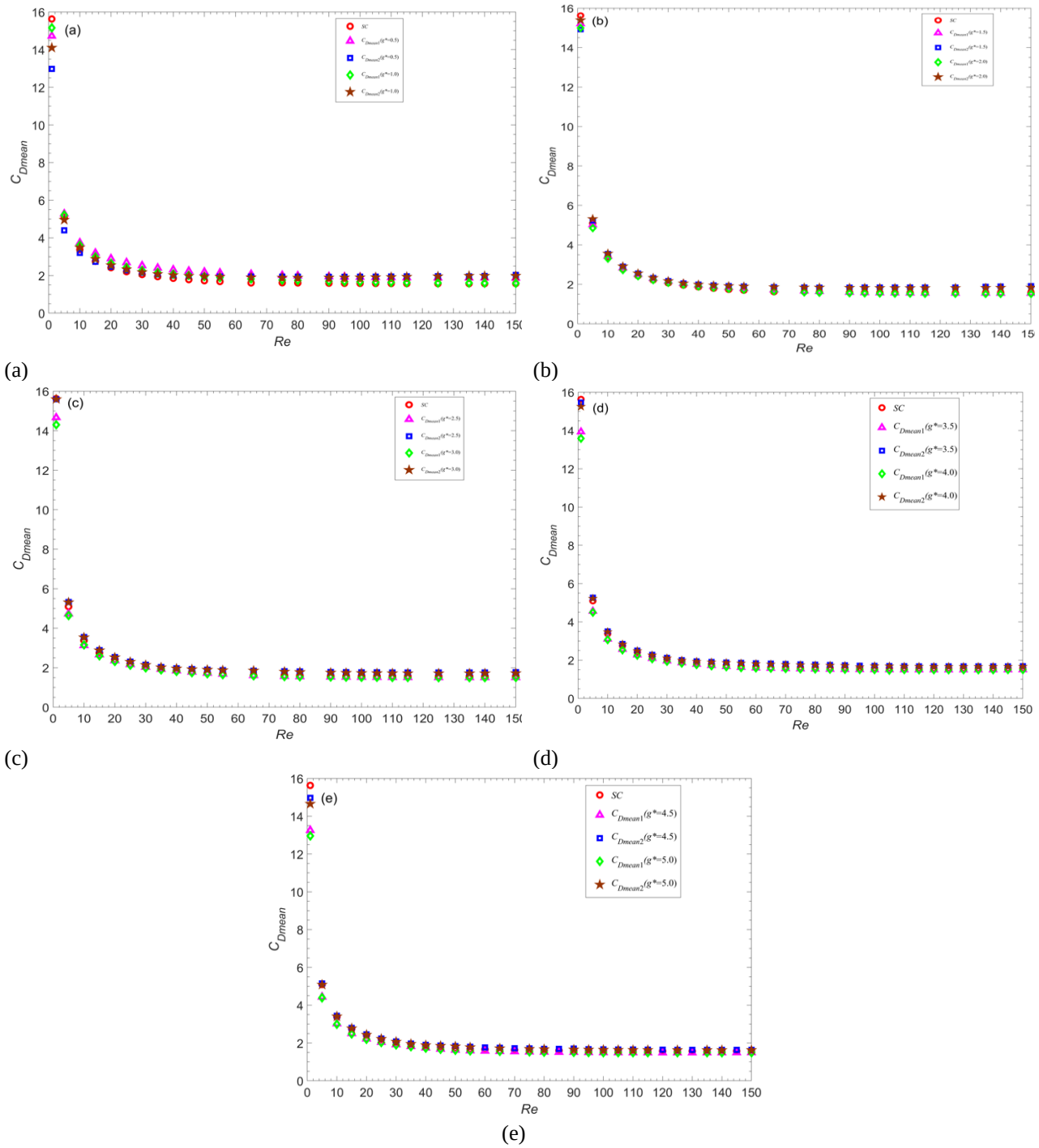

Fig. 15 Variation of mean drag coefficients with different spacing ratio from 0.5 to 5

cylinders are higher than single cylinder. After showing constant behavior up to $Re = 35$ the C_{Drms2} values exhibit higher values than that of C_1 and SC (Fig. 16(c)). The major change that we observe from Fig. 16(c) is that for $Re \geq 110$ both C_1 and SC shows same values of C_{Drms}. Moreover, in Fig. 16(d, e) same as previous graphs of C_{Drms} the values of C_{Drms2} are higher from C_{Drms1}, and it can be observed that C_{Drms} value of SC is higher than that of C_{Drms1} in previous graphs these values were lower or equal. Increasing in g^* between cylinders results in decreasing of C_{Drms} values. C_{Drms} values of C_2 are higher than $C_1$and for $g^* \geq 3.5$ the values of C_1 are lower than single SC (Fig. 16(a-e)).

C_{Lrms} variation of Re at various g^* from 0.5 to 5 are presented in Fig. 17(a-e). We did not observe observed C_{Lrms} values for steady flow in initials Re from 1 to 30, for small g^* transition starts ta $Re = 35$ and for large g^* transition starts at $Re = 40$. C_{Lrms} values of C_2 are higher than that of C_1 which means that C_2 is facing highest lift force and it can be also noticed that for $Re \geq 80$ the SC values are higher than C_1 and are lower than C_2 (Fig. 17(a)). At $g^*= 0.5$ and 1 the C_{Lrms} values of SC are closer to C_1 than C_2 and we can also observe a notable difference between C_{Lrms} values of both cylinder which indicates irregularities in flow. In Fig. 17(b) C_{Lrms} values

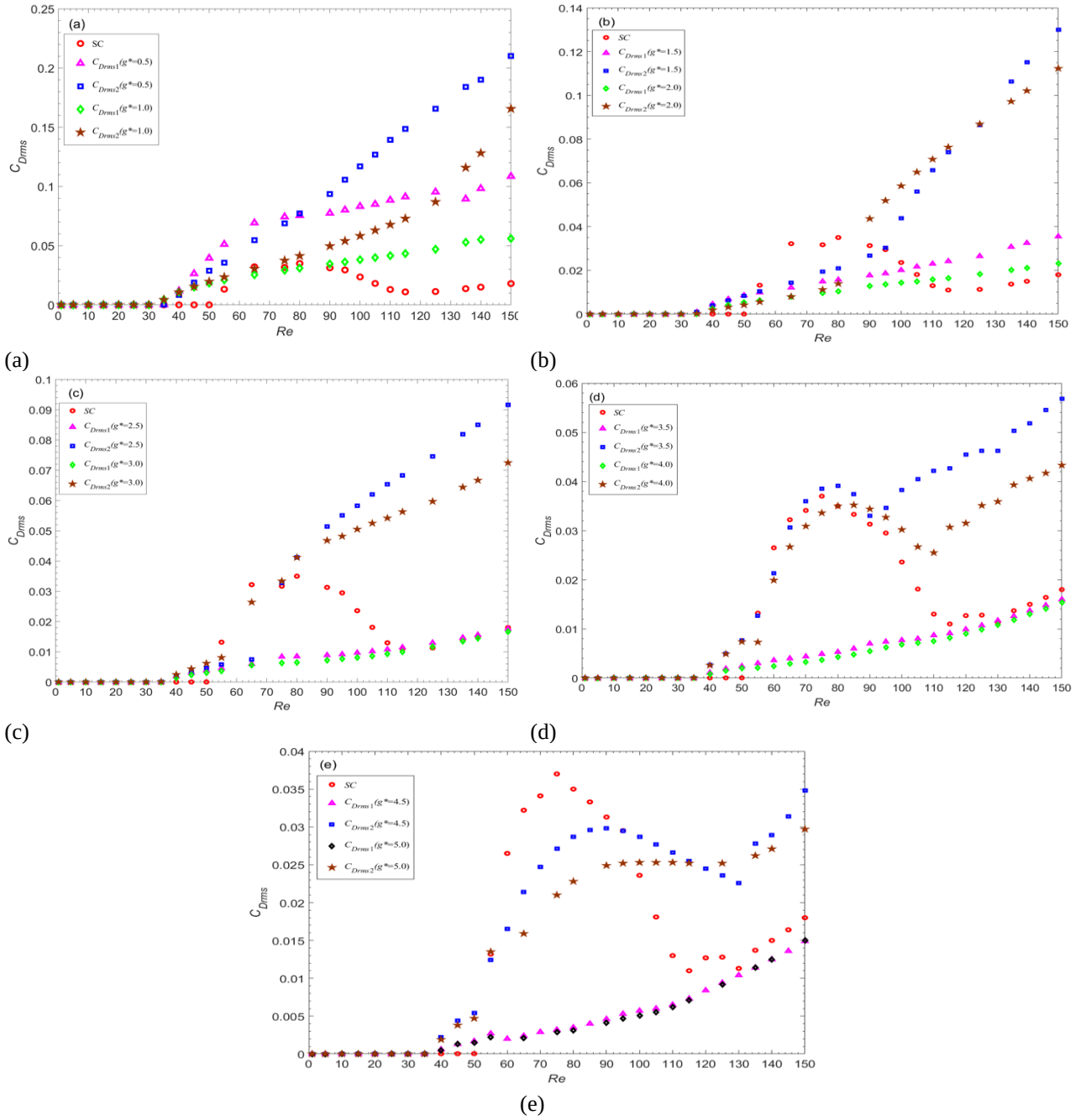

Fig. 16 Investigation of variation of root-mean square values with different spacing ratio from 0.5 to 5

are increasing with increment in Re, C_{Lrms2} values of both cylinders become closer to each and same in the case of C_{Lrms1} values, SC C_{Lrms} values lies between C_{Lrms1} and C_{Lrms2} values of both cylinders and almost have same distance up to $Re = 80$ and then it becomes more closer to C_{Lrms1}. We can see that C_{Lrms} values of C_2 are higher than C_1 and SC at both $g^* =$ 2.5 and 3, and SC values lie between them (Fig. 17(c)). In Fig. 17(d, e) it can be notice that C_{Lrms} values of both C_1 and C_2 show same behavior, which means that at large g^* flow is fully developed and regular. The C_{Lrms} values of C_2 are higher than SC and C_1, and C_{Lrms} values of C_1 are lower than SC which clearly demonstrate that the effect C_2 results in increase of C_L.

Figure 18(a-e) demonstrates the different variation of St with Re at different gap spacing from 0.5 to 5 with 0.5 increment. Fast Fourier Transform (FFT) command is applied on C_L for calculation of St, which is built-in command of MATLAB, usually St is used for indication of vortex shedding frequency. As we know that for steady flow constant behavior is observed for C_L and as a result there is no St values for steady flow state. In Fig. 18(a-e) St values for unsteady and transitional cases are presented. It is also observed that for small g^* from 0.5 to 2 is the flow transition is started at $Re = 35$, and on the other hand for large g^* from 2.5 to 5, $Re = 40$ is the starting point for transitional flow. The St values of SC are higher than St_1 and St_2 (Fig. 18(a)). Moreover, St values of both cylinder at $g^* = 1$ is higher as compared to St values at $g^* =$ 0.5, and we are unable to predict the behavior of St values

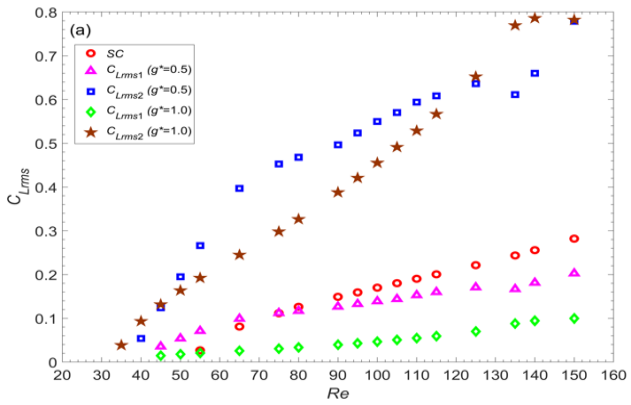

(a) C_{Lrms} with Re at different g* from 0.5 to 5

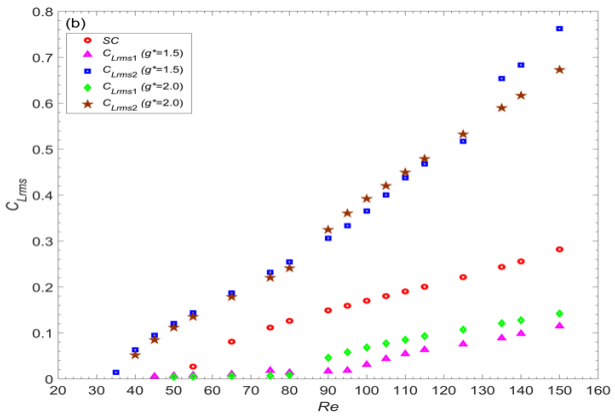

(b) C_{Lrms} with Re at different g* from 0.5 to 5

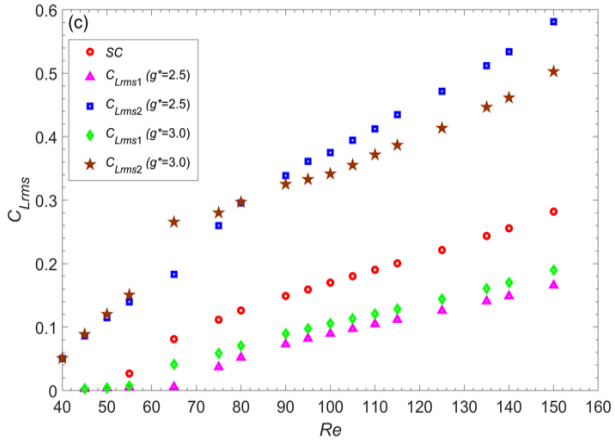

(c) C_{Lrms} with Re at different g* from 0.5 to 5

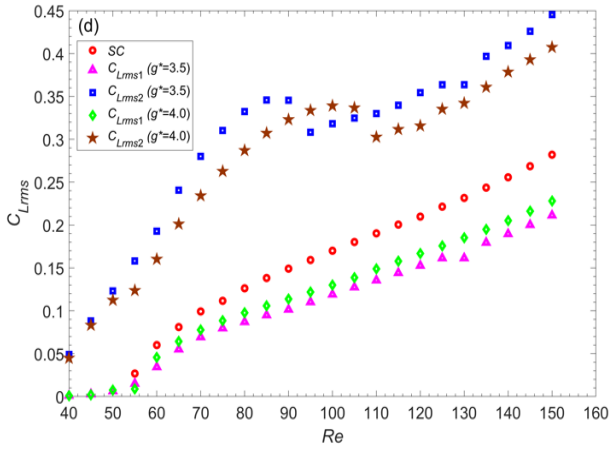

(d) C_{Lrms} with Re at different g* from 0.5 to 5

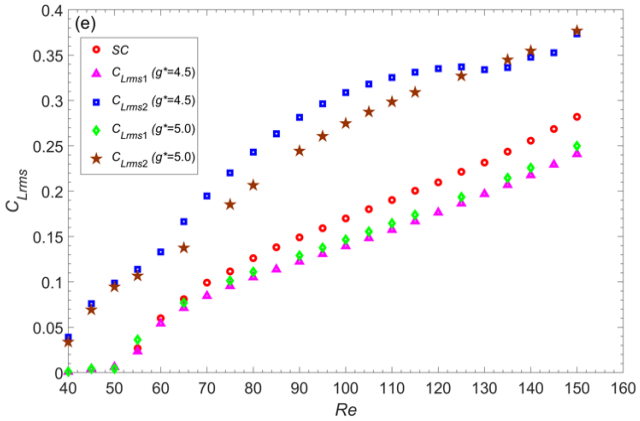

(e) Variation of C_{Lrms} with Re at different g* from 0.5 to 5

Fig. 17 Investigation of variation of C_{Lrms} with Re at different g* from 0.5 to 5

because they are not increasing or decreasing in a proper way, and abrupt changes in their behavior is observed. This behavior is due to the strong wake interaction because of small g^* (Fig. 18(a)). It can be notice from Fig. 18(b) that the $St_1$of both cylinders are higher than SC and that of St_2, and St values of C_2 are lower than SC. We can see that up to $Re = 80$ there is small difference between St values and after that we noticed notable change in their values which shows that flow is more complex at downstream position than upstream position (Fig. 18(b)). Almost same behavior can be seen in Fig. 18(c), but St values are closer to each other as compared to previous graphs. At large g^*, St values of both C_1 and C_2 and as well as SC almost shows same behavior and there is not that much difference in their values which means that flow is developed, and such type of flow is an example of In-phase flow pattern (Fig. 18(d, e)). Overall, we can deduce that with increasing gap spacing results in development of flow.

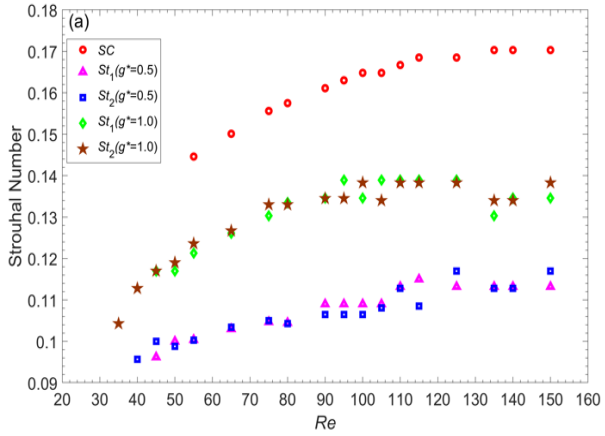

(a) St along with various spacing ratio from 0.5 to 5

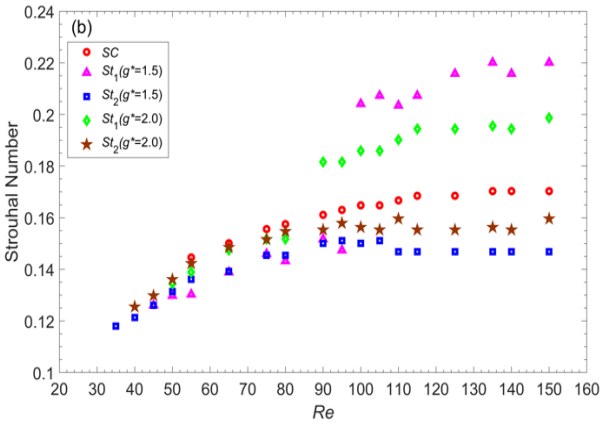

(b) St along with various spacing ratio from 0.5 to 5

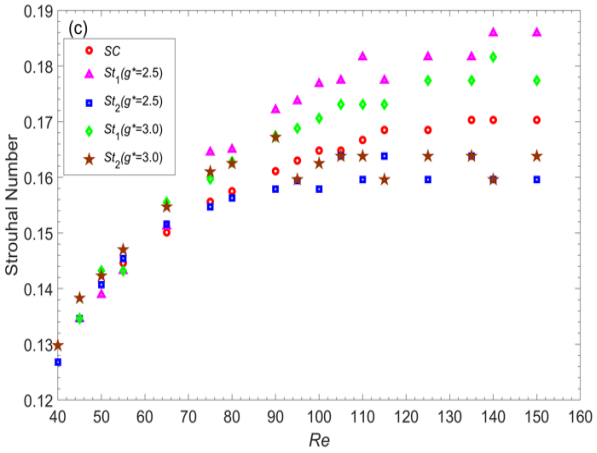

(c) St along with various spacing ratio from 0.5 to 5

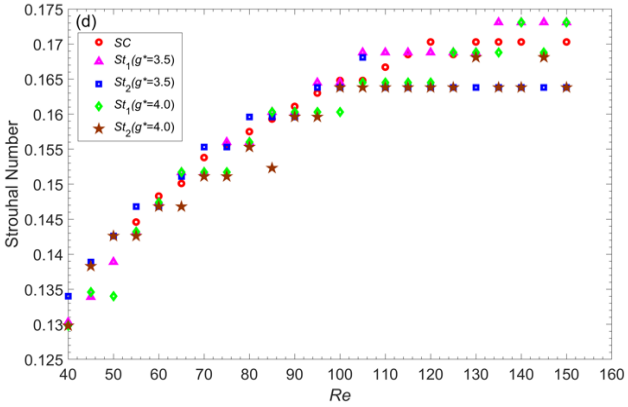

(d) St along different spacing ratio from 0.5 to 5

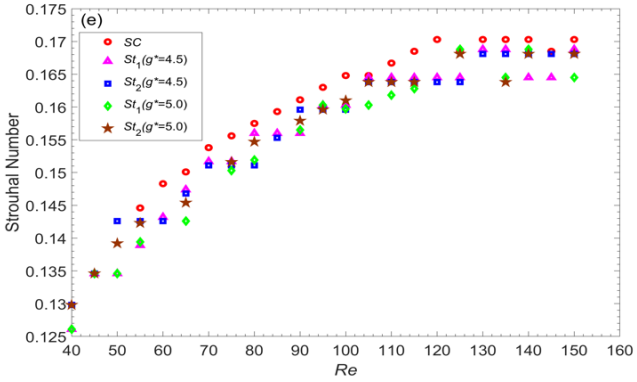

(e) St with different spacing ratio from 0.5 to 5

Fig. 18 Variation of St along with various spacing ratio from 0.5 to 5

5. RESULTS DISCUSSION AND COMPARISON

We have learned a great deal about the complex dynamics of fluid flow from our study of the flow characteristics behind square offset cylinders with varying gap and Reynolds numbers. One of the key findings is the significant influence of Reynolds numbers on the observed flow patterns. Higher Reynolds numbers cause the flow behind the cylinders to become more complicated, exhibiting increased flow separation and vortex shedding. Conversely, flow patterns with lower Reynolds numbers are more regular and consistent. These results are consistent with prior studies in the field and recognized theories of fluid dynamics. Further analysis of the flow behavior at different gap spacings shows the appearance of different flow patterns.

Smaller gap spacings frequently promote more complicated interactions, which may enhance fluid mixing and perhaps change the wake shape. Our study advances our understanding of the flow dynamics behind cylinders and how Reynolds numbers and gap spacings affect it, which is important for many engineering applications to

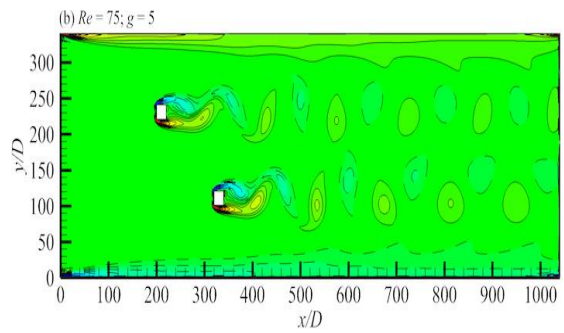

(a) For $Re = 75$ and $g^*= 5.0$

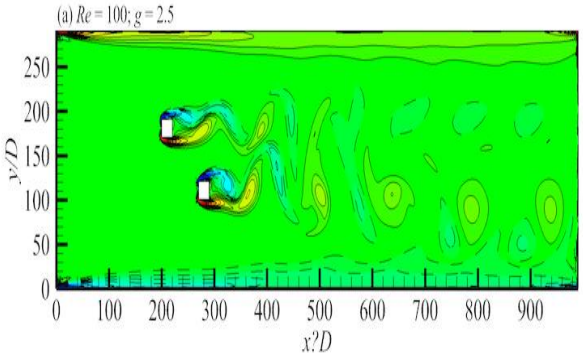

(b) For $g^*= 2.5$ and $Re = 100$

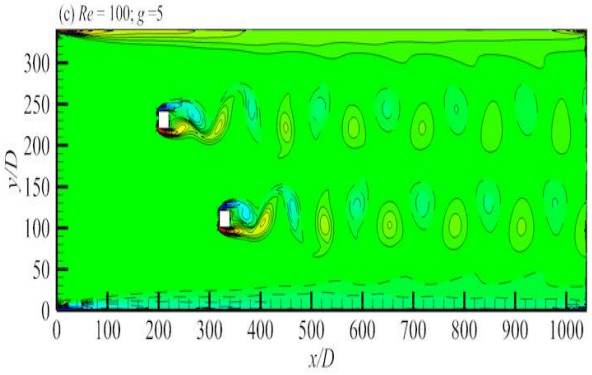

(c) For $Re = 100$ and $g^*= 5.0$

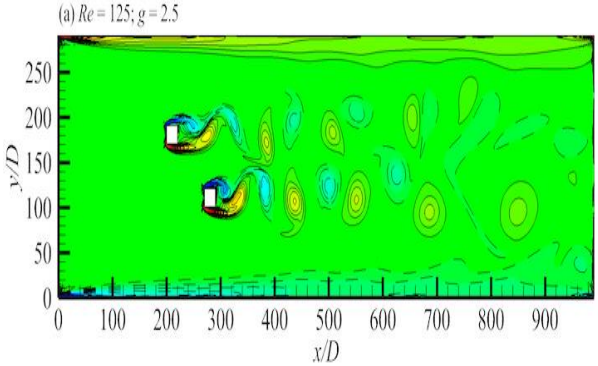

(d) For $g^*= 2.5$ and $Re = 125$

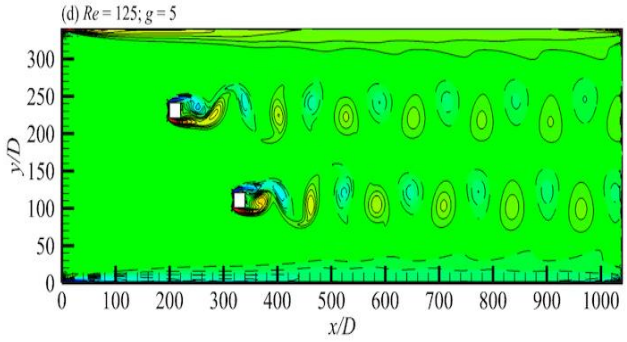

(e) For $g^*= 5$ and $Re = 125$

Fig. 19 Vorticity flow through two offset square cylinders at varying g^* and Re is visualized contour-wise

work as well as possible. All in all, our findings align with previous research on fluid mechanics.

In Table 5, the authors have presented a thorough comparison of their findings with previously released data for Re = 150. This makes it possible to compare the present results in depth. The current study's result for the mean drag coefficient (CDmean) was 1.6170, which is in good accord with the results of numerous other investigations that reported values between 1.4501 and 1.6680. The present outcome is situated squarely in the center of this range. The current value is larger than that of An et al. (2020) and Alam et al. (2016), the two most recent research, but it is lower than the latter.

The current analysis yielded a Strouhal number (St) of 0.1745. This is in good agreement with other earlier investigations that showed Strouhal numbers at Re = 150 ranging from 0.1579 to 0.1751. Once more, the current outcome fits well into the spectrum of data that has been released. It is marginally lower than Furquan and Mittal (2015), but marginally higher than the values given by Sharma and Eswaran (2004) and Aboueian and Sohankar (2017). The current result of 0.2847 for the rms lift coefficient (CLrms) is extremely similar to the value of 0.2850 found by Saha et al. (2003). Additionally, it concurs with findings in Singh's et al. (2021) and Alam et al. (2016), which are 0.2741 and 0.2781, respectively. The current CLrms is marginally more than the value of 0.2401 that Aboueian and Sohankar (2017) reported.

He results obtained in the current study for CDmean, St, and CLrms at Re = 150 show good agreement with previous published data. The values generally fall within the ranges reported in the literature. This provides validation for the lattice Boltzmann simulation method and modeling approach used by the authors. The comprehensive comparison in Table 5 allows for an in-

Table 5 Thorough examination of current data and findings for the Reynolds number of 150

Researchers	C_{Dmean}	St	$Drms$	C_{Lrms}
Robichuax et al. (1999)	1.6680	0.1631	⋯	⋯
Alam et al. (2016)	1.4537	0.1678	0.0178	0.2781
Liu and Jaiman (2016)	⋯	0.1601	⋯	⋯
An et al. (2020)	1.4501	0.1631	⋯	⋯
Furquan and Mittal (2015)	1.650	0.1751	⋯	⋯
Shimizu and Tanida (1978)	1.5800	⋯	⋯	⋯
Saha et al. (2003)	1.6200	0.1641	0.00180	0.2850
Singh et al. (2016)	1.6000	0.1665	⋯	0.2741
Sharma and Eswaran (2004)	1.5568	0.1579	0.0195	0.2913
Chatterjee et al. (2010)	⋯	0.1697	⋯	⋯
Aboueian and Sohankar (2017)	1.5300	0.1551	⋯	0.2401
Norberg (1993)	⋯	0.1471	⋯	⋯
Proposed study results	1.6170	0.1745	0.0185	0.2847

depth assessment of how the present results fit with existing knowledge.

Compared to prior investigations of flow around circular cylinders at similar Reynolds numbers, several similarities and differences are noted in the wake behaviors with square cylinders in the present offset arrangement. The onset of vortex shedding indicates the transition from steady flow to unsteadiness occurs at comparable Reynolds number ranges in both circular and square configurations, suggesting some universality. However, the initial shedding modes tend to be more irregular and disorganized with square geometries.

Additionally, the critical spacing ratio to achieve a fully developed wake appears to be higher for the square cylinders compared to typical values reported for circular cylinders.

These distinctions likely arise because the sharp corners of the square geometry promote flow separation and the development of complex turbulent stresses in near wake. Bluffer body shapes are more prone to exhibiting a wider variety of wake modes. However, at sufficient spacing ratios where the wakes do not interact or merge significantly, similarities in periodic vortex shedding behavior start to emerge between circular and square cases. The key forces statistics like Strouhal number, drag, and lift coefficients also differ quantitatively between circular and square cylinders, but the overall qualitative trends with respect to Reynolds number and spacing ratio variations follow comparable progression patterns. In summary, despite some unique phenomena promoted by the square geometry and orientation, the fundamental wake transition behaviors share similarities with classical circular cylinder arrangements when considering parameter variations. This points to potential universal criteria governing the process of wake development behind bluff body obstacles. Further comparative analyses can provide more detailed delineation of geometry-specific effects.

6. CONCLUSION

A two-dimensional method type of the lattice Boltzmann based on the single-relaxation-time is applied to study the flow features and force statistics analysis behind two square offset cylinders at various Reynolds numbers and spacing ratios and key findings are presented. Reynolds numbers have been found to have a significant impact on flow behind cylinders and different flow patterns and behaviors for various gap spacing types and Reynolds values are noted. The following is the summary of the main conclusion:

From $Re = 1$ to 30 and for all g* steady flow with no transition is observed in the whole computational domain.

It is found that with increasing Re results in increasing the recirculation length and flow remain steady. $Re = 35$ is the starting point of vortices generation behind downstream cylinder and quasi steady flow is noticed behind upstream cylinder and vortices starts generating behind upstream cylinder at $Re = 40$ at small gap spacing and for large gap spicing flow is quasi unsteady up to $Re = 40$. Different type of flow regime is observed: (a) steady flow regime, also part (b) that single-bluff style of body flow regime, (c) chaotic flow regime, (d) flip-flopping flow regime and fully developed flow regime is observed depending on different Re and spacing. It is also notice that Re and spacing has a huge impact on flow behind offset square cylinders and low spacing complexity and irregularities occurs in flow pattern behind cylinder due to jet flow whereas increasing in spacing flow advance through developing stages and we can observe two rows fully developed flow regime. The C_{Dmean} values are higher at $Re = 1$ and then sudden decreasing jump is observed, and it show relatively small values ate $Re = 5$ because of inertial forces and minor decreasing trend with increasing Re is observed up to $Re = 55$ because of weaker viscous force which results in weaker C_D and then constant behavior is observed up to $Re = 150$.

In C_{Lrms} plots it is seen that C_{Lrms1} and C_{Lrms2} are distant apart from each other and from single cylinder at behave differently which is the sign of irregularities and modulated signals whereas at large spacing the distance between C_{Lrms1} and C_{Lrms2} values is reduced and behave likely, and single cylinder values are more closer to C_{Lrms1} which means that the amplitude of modulation of downstream cylinder is higher than upstream cylinder.

The use of a two-dimensional lattice Boltzmann based on the time for single relaxation approach has demonstrated the major influence of numbers named as Reynolds on flow patterns behind square offset cylinders with a range of gap spacings. This study proposes several exciting new directions. The study's three-dimensional modelling extension, investigation of turbulence transitions, application of the research to actual engineering issues, advancement of numerical methods, experimental validation of the findings, and integration of multi-physics simulations are a few of these. By pursuing these paths, we can broaden our understanding of fluid dynamics and its practical applications in science and engineering.

For more physical interpretation of why different flow phenomena are observed under varying conditions:

- Consistent flow at low Reynolds numbers: At very low Reynolds numbers, viscous forces—rather than inertial forces—dominate the flow. This allows the boundary layer to remain attached and not separate. Therefore, no unsteadiness or vortex shedding occurs, resulting in a steady flow pattern.
- Onset of unsteadiness at moderate Re - As Re increases, inertial forces start becoming more significant compared to viscous forces. This causes the boundary layer to detach from the cylinder surfaces, resulting in flow separation and vortex shedding in the wake. This marks the onset of unsteady flow phenomena.
- Chaotic flows at smaller spacings - When there is little space between the cylinders, the interacting shear layers, and proximity of the wakes causes highly chaotic and turbulent mixing. Vortices shed by one cylinder impinge on the other cylinder in an unpredictable manner, leading to aperiodic forces and lack of an organized pattern.
- Flip-flopping flows at moderate spacings - At moderate spacings, the wakes have some freedom to develop but still interfere with each other. Flip-flopping, or the occasional shifting of the wake width from one side to the other, results from this. The forces switch between different quasi-periodic modalities rather than having a single frequency.
- Fully developed flow at higher spacings - As spacing increases further, the wakes have enough room to fully develop in a manner like isolated cylinders. This allows the typical von Karman vortex street pattern, with vortices shed from each cylinder interacting very little. A single dominant shedding frequency emerges in a stable periodic pattern.
- Overall, from Re = 1 to 30, the flow remains attached to the cylinders, and it is steady behind both cylinders. At Re>35, vortices are observed to be generated behind both cylinders, with the first one occurring downstream of the cylinder. When there is less gap spacing, the flow behind both cylinders' mixes, exhibiting chaotic and turbulent behavior. However, for higher gap spacing, the flow does not mix, and Von-Karman vortex shedding is observed behind both cylinders.

This provides the insight into the physical mechanisms behind why the flow regimes transition in the manner observed in this study.

ACKNOWLEDGEMENTS

The Petchra Pra Jom Klao Ph.D. has been awarded a research fellowship by King Mongkut's University of Technology Thonburi (KMUTT) under Grant No. (49/2565) to fund this research. The Unit for Human Resources & Institutional Development, Research, Program Management and Innovation [grant number B39G660025] Thailand on behalf of the NSRF has provided funding assistance for this innovative study.

CONFLICT OF INTEREST

The authors have no conflicts to disclose.

AUTHORS CONTRIBUTION

All the authors have equally contributed. **S. Ul-Islam** was responsible for the initial conceptualization of the study. **M. Abid** was responsible for design of the research methodology, and the thorough analysis of the simulation results and final writing of the draft. **N. Yasin** was instrumental in developing the computational software necessary for the lattice Boltzmann simulations. **S. Ahmad** was responsible for executing the numerical simulations using the lattice Boltzmann method and validating the results through rigorous testing. **M. Saqlain** critically reviewed and edited the manuscript, providing valuable insights and improvements to the content. He supervised the research process and were responsible for securing the funding necessary to conduct the study."

REFERENCES

Abdulaziz, K. G. A., Mohammed, K. A., Saima, R., & Muhammad, A. (2022). A novel numerical treatment of nonlinear and nonequilibrium model of gradient elution chromatography considering core-shell particles in the column. *Mathematical Problems in Engineering, 2022*, 1619702–1619702. https://doi.org/10.1155/2022/1619702

Abid, M., Bibi, M., Yasin, N., & Shahid, M. (2024). A Novel computational analysis of boundary driven two-dimensional heat flow with the internal heat generation. *Computational Algorithms and Numerical Dimensions*. http://dx.doi.org/10.22105/cand.2024.443017.1090

Aboueian, J., & Sohankar, A. (2017). Identification of flow regimes around two staggered square cylinders by a numerical study. *Theoretical and Computational Fluid Dynamics, 31*(3), 295–315. https://doi.org/10.1007/s00162-017-0424-2

Aboueian, J., Sohankar, A., Rastan, M. R., & Ghodrat, M. (2021). An experimental study on flow over two finite wall-mounted square cylinders in a staggered arrangement. *Ocean Engineering, 240*, 109954-

109954. https://doi.org/10.1016/j.oceaneng.2021.109954

Alam, M. M., Bai, H., & Zhou, Y. (2016). The wake of two staggered square cylinders. *Journal of Fluid Mechanics*, *801*, 475–507. https://doi.org/10.1017/jfm.2016.303

An, B., Bergada, J. M., Mellibovsky, M., Sang, W. M., & Xi, C. (2020). Numerical investigation on the fow around a square cylinder with an upstream splitter plate at low Reynolds numbers. *Meccanica*, *55*, 1037–1059. https://doi.org/10.1007/s11012-020-01148-8

Bai, X. D., Zhang, W., & Wang, Y. (2020). Deflected oscillatory wake pattern behind two side-by-side circular cylinders. *Ocean Engineering*, *197*, 106847–106847. https://doi.org/10.1016/j.oceaneng.2019.106847

Baranwal, A. K., & Chhabra, R. P. (2016). Free convection in confined power-law fluids from two side-by-side cylinders in a square enclosure. *Heat Transfer Engineering*, 37(18), 1521–1537. https://doi.org/10.1080/01457632.2016.1151296

Bhatnagar, P. L., Gross, E. P., & Krook, M. (1954). A model for collision processes in gases. I. Small amplitude processes in charged and neutral one-component systems. *Physical Review*, *94*(3), 511–511. https://doi.org/10.1103/PhysRev.94.511

Chatterjee, D., Biswas, G., & Amiroudine, S. (2010). Numerical simulation of flow past row of square cylinders for various separation ratios. *Computers & Fluids*, *39*, 49–59. https://doi.org/10.1016/j.compfluid.2009.07.002

Chen, W., Ji, C., Xu, D., & Srinil, N. (2019). Wake patterns of freely vibrating side-by-side circular cylinders in laminar flows. *Journal of Fluids and Structures*, *89*, 82–95. https://doi.org/10.1016/j.jfluidstructs.2019.02.013

Dou, H., Zhang, S., Yang, H., Setoguchi, T., & Kinoue, Y. (2018). Effect of rotational speed on the stability of two rotating side-by-side circular cylinders at low reynolds number. *Journal of Thermal Science*, *27*(2), 125–134. https://doi.org/10.1007/s11630-018-0993-4

Furquan, M., & Mittal, S. (2015). Flow past two square cylinders with flexible splitter plates. *Computational Mechanics*, *55*(6), 1155–1166. https://doi.org/10.1007/s00466-014-1110-5

Griffith, M. D., Jacono, D. L., Sheridan, J., & Leontini, J. S. (2017). Flow-induced vibration of two cylinders in tandem and staggered arrangements. *Journal of Fluid Mechanics*, *833*, 98–130. https://doi.org/10.1017/jfm.2017.673

Guo, Z. L., & Shu, C. (2013). *Lattice boltzmann method and its applications in engineering*. World Scientific Publishing Co. Pte. Ltd., Singapore. http://dx.doi.org/10.1142/8806

Haq, H. B. U., Akram, W., Irshad, M. N., Kosar, A., & Abid, M. (2024). Enhanced real-time facial expression recognition using deep learning. *Acadlore Transactions on AI and Machine Learning (ATAIML)*, *3*(1), 24-35. http://dx.doi.org/10.56578/ataiml030103

Hsu, L. C., Chen, C. L., & Ye, J. Z., (2017). A study of flow patterns for staggered cylinders at low Reynolds number by spectral element method. *Journal of Mechanical Science and Technology*, *31*(6), 2765–2780. https://doi.org/10.1007/s12206-017-0520-7

Islam, S. U., Nazeer, G., & Shigri, S. H., (2019). Numerical investigation of different flow regimes for square cylinders in staggered configuration. *KSCE Journal of Civil Engineering*, *23*(5), 2188–2197. https://doi.org/10.1007/s12205-019-0726-6

Kim, S., & Alam, M. M. (2015). Characteristics and suppression of flow-induced vibrations of two side-by-side circular cylinders. *Journal of Fluids and Structures*, *54*, 629–642. https://doi.org/10.1016/j.jfluidstructs.2015.01.004

Krüger, T., Kusumaatmaja, H., Kuzmin, A., Shardt, O., Silva, G., & Viggen, E. M. (2017). The lattice Boltzmann method. *Springer International Publishing*, *10*(978-3), 4-15. https://doi.10.1007/978-3-319-44649-3

Liu, B., & Jaiman, R. K. (2016). *The effect of gap flow on vortex-induced vibration of side-by-side cylinder arrange- ment.* International Conference on Offshore Mechanics and Arctic Engineering. https://doi.org/10.1115/OMAE2016-54736

Meneghini, J. R., Saltara, F., Siqueira, C. L. R., & Ferrari, J. A. (2001). Numerical simulation of flow interference between two circular cylinders in tandem and side-by-side arrangements. *Journal of fluids and structures*, *15*(2), 327–350. https://doi.org/10.1006/jfls.2000.0343

Mohamad, A. A. (2011). *Lattice Boltzmann Method*. Springer, London. https://doi.org/10.1007/978-1-4471-7423-3

Muhammad, A. A. (2019). *Lattice Boltzmann method: fundamental and engineering applications with computer codes*. Springer, New York. https://doi.org/10.2514/1.J051744

Murtaza, S. & Ahmad, Z. (2024). Analysis of Clay Based Cementitious Nanofluid Subjected to Newtonian Heating and Slippage Conditions with Constant Proportional Caputo Derivative. GeoStruct Innovations (GSI), 2(2), 53-67. https://doi.org/10.56578/gsi020201

Norberg, C. (1993). Flow around rectangular cylinders: pressure forces and wake frequencies. *Journal of Wind Engineering and Industrial Aerodynamics*, *49*, 187–196. https://doi.org/10.1016/0167-6105(93)90014-F

Octavianty, R., & Asai, M. (2016). Effects of short splitter plates on vortex shedding and sound generation in flow past two side-by-side square cylinders. *Experiments in Fluids*, *57*(9), 1–13.

https://doi.org/10.1007/s00348-016-2227-4

Patel, C. G., Sarkar, S., & Saha, S. K. (2018). Mixed convective vertically upward flow past side-by-side square cylinders at incidence. *International Journal of Heat and Mass Transfer*, *127*, 927–947. https://doi.org/10.1016/j.ijheatmasstransfer.2018.06.129

Rashidi, S., Keimanesh, M., & Khanjani, M. (2020). Numerical study of entropy generation in heat transfer from tandem square cylinders. *International Journal of Thermal Sciences*, *154*, 106460. https://doi.org/10.1016/j.ijthermalsci.2020.106460

Rehman, N., Abid, M., & Qamar, S., (2021). Numerical approximation of nonlinear and non-equilibrium model of gradient elution chromatography. *Journal of Liquid Chromatography & Related Technologies*, *44*(7-8), 382-394,. https://doi.org/10.1080/10826076.2021.1947316

Robichuax, J., Balachandar, S., & Vanka, S. P. (1999). Three-dimensional floquet instability on the wake of square cylinder. *Physics of Fluids*, *11*(2-3), 560-578. https://doi.org/10.1063/1.869930

Saha, A. K., Biswas, G., & Muralidhar, K. (2003). Three-dimensional study of fow past a square cylinder at low Reynolds numbers. *International Journal of Heat and Fluid Flow*, *24*, 54–66. https://doi.org/10.1016/S0142-727X(02)00208-4

Sanyal, A., & Dhiman, A. (2020). Shear-induced viscosity stratified flow past a pair of heated side-by-side square cylinders in a confined domain. *Physics of Fluids*, *32*(5), 53601-53601. https://doi.org/10.1063/5.0002083

Saqlain, M., Abid, M., Awais, M., & Stević, Ž. (2024). Analysis of software effort estimation by machine learning techniques. *Ingénierie des Systèmes d'Information,* *28*, 1445-1457. http://dx.doi.org/10.18280/isi.280602

Sharma, A., & Eswaran, V. (2004). Heat and fluid flow across a square cylinder in the two-dimensional laminar flow regime. *Numerical Heat Transfer, Part A: Applications*, *45*(3), 247-269. https://doi.org/10.1080/10407780490278562

Sharma, A., Raj, C. T., Chhabra, R. P., & Sharma, A. (2021). Machine learning modeling for wake turbulence downstream of a wall-mounted square cylinder. *Physics of Fluids*, *33*(11), 115118. https://doi.org/10.1063/5.0063967

Shen, Z., Chen, Z., Xiang, N., Zong, W., & Tian, F. (2021). Numerical investigation and modal analysis of flow past two staggered circular cylinders. *Physics of Fluids*, *33*(8), 085110. https://doi.org/10.1063/5.0058258

Shimizu, Y., & Tanida, Y., (1978). Fluid forces acting on cylinders of rectangular cross-section. *Transactions of the Japan Society of Mechanical Engineers-B*, *44*, 2699–2706. https://doi.org/10.11159/jffhmt.2020.004

Singha, S., Nagarajan, K. K., & Sinhamahapatra, K. P. (2016). Numerical study of two-dimensional flow around two side-by-side circular cylinders at low Reynolds numbers. *Physics of Fluids*, *28*(5), 53603–53603. https://doi.org/10.1063/1.4949332

Tong, F., Cheng, L., & Zhao, M. (2015). Numerical simulations of steady flow past two cylinders in staggered arrangements. *Journal of Fluid Mechanics*, *765*, 114-149. https://doi.org/10.1017/jfm.2014.708

Veena, V., Muddada, S., & Eldho, T. I. (2020). Flow-induced vibration characteristics of elastically mounted rigid square cylinders in tandem arrangements. *Journal of Fluids and Structures*, *100*, 103149. https://doi.org/10.1016/j.jfluidstructs.2020.103149

Vinodh, A., & Supradeepan, K. (2020). A numerical study on influence of the control cylinder on two side-by-side cylinders. *Journal of the Brazilian Society of Mechanical Sciences and Engineering*, *42*(4), 1–12. https://doi.org/10.1007/s40430-020-2264-z

Vu, H. C., Ahn, J., & Hwang, J. H. (2016). Numerical simulation of flow past two circular cylinders in tandem and side-by-side arrangement at low Reynolds numbers. *KSCE Journal of Civil Engineering*, *20*(4), 1594–1604. https://doi.org/10.1007/s12205-015-0602-y

Wolf-Gladrow, D. A. (2004). *Lattice-gas cellular automata and lattice Boltzmann models: an introduction.* Springer. https://doi.org/10.1007/b72010

Woyciekoski, M. L., Endres, L. A. M., Paula, A. V. D., & Mo¨ller, S. V. (2020). Influence of the free end flow on the bistability phenomenon after two side by side finite height cylinders with aspect ratios of 3 and 4 and high blockage. *Ocean Engineering*, *195*, 106658–106658. http://dx.doi.org/10.1016/j.oceaneng.2019.106658

Wu, G., Du, X., & Wang, Y. (2020). LES of flow around two staggered circular cylinders at a high subcritical Reynolds number of 1.4× 105. *Journal of Wind Engineering and Industrial Aerodynamics*, 104044–104044. https://doi.org/10.1016/j.jweia.2019.104044

Wu, X. D., Liu, H. P., & Chen, F. (2018). Numerical investigation of flow characteristics around two side-by-side cylinders by immersed boundary-lattice Boltzmann flux solver. *Journal of Zhejiang University-Science A*, *19*(5), 384–398. 384–398. http://doi.org/10.1631/jzus.A1700112

Xu, W., Qin, W., & Yu, Y. (2020). Flow-induced vibration of two identical long flexible cylinders in a staggered arrangement. *International Journal of Mechanical Sciences*, *180*, 105637–105637. https://doi.org/10.1016/j.ijmecsci.2020.105637

Zhang, C., Kang, Z., Xiong, Y., Ai, S., & Ma, G., (2021). Experimental investigation on coupled crossflow and in-line vortex-induced vibration responses of two staggered circular cylinders. *Proceedings of the Institution of Mechanical Engineers*, *235*, 288–300.

https://doi.org/10.1177/1475090220907473

Zhang, W., Li, X., and Zhu, Z., (2019). Quantification of wake unsteadiness for low-Re flow across two staggered cylinders. *Proceedings of the Institution of Mechanical Engineers, 233*, 6892–6909. https://doi.org/10.1177/0954406219866478

Zhang, Y., Sheng, L., Duan, J., Chen, K., & You, Y., (2018). *LBM simulation of flow around an oscillating cylinder and a stationary cylinder in side-by-side arrangement.* International Conference on Offshore Mechanics and Arctic Engineering. https://doi.org/10.1115/OMAE2018-77133

Zhou, C. Y. (2021). Flow control around two side-by-side square cylinders using dual splitter plates. *Journal of the Brazilian Society of Mechanical Sciences and Engineering, 43*(2), 1–28. https://doi.org/10.1007/s40430-020-02795-4

Zhou, Y., Nagata, K., Sakai, Y., Watanabe, T., Ito, Y., & Hayase, T. (2020). Energy transfer in turbulent flows behind two side-by-side square cylinders. *Journal of Fluid Mechanics*, 903–903. https://doi.org/10.1017/jfm.2020.611

Zhou, Y., Wang, Z., Qian, Y., Yang, H., & Wei, Y., (2021). Numerical simulation of the flow around two square cylinders using the lattice Boltzmann method. *Physics of Fluids, 33*(3), 37110–37110. https://doi.org/10.1063/5.0040020